

Review

Low Pt Alloyed Nanostructures for Fuel Cells Catalysts

Shuoyuan Huang ^{1,†}, Aixian Shan ^{2,†} and Rongming Wang ^{1,*}

¹ Beijing Advanced Innovation Center for Materials Genome Engineering, Beijing Key Laboratory for Magneto-Photoelectrical Composite and Interface Science, School of Mathematics and Physics, University of Science and Technology Beijing, Beijing 100083, China; syhuang443@gmail.com

² Center for Green Innovation, School of Mathematics and Physics, University of Science and Technology Beijing, Beijing 100083, China; sax2005@163.com

* Correspondence: rmwang@ustb.edu.cn; Tel.: +86-010-62332354

† These authors contributed equally to this work.

Received: 22 October 2018; Accepted: 4 November 2018; Published: 13 November 2018



Abstract: Low-noble metal electrocatalysts are attracting massive attention for anode and cathode reactions in fuel cells. Pt transition metal alloy nanostructures have demonstrated their advantages in high performance low-noble metal electrocatalysts due to synergy effects. The basic of designing this type of catalysts lies in understanding structure-performance correlation at the atom and electron level. Herein, design threads of highly active and durable Pt transition metal alloy nanocatalysts are summarized, with highlighting their synthetic realization. Microscopic and electron structure characterization methods and their prospects will be introduced. Recent progress will be discussed in high active and durable Pt transition metal alloy nanocatalysts towards oxygen reduction and methanol oxidation, with their structure-performance correlations illustrated. Lastly, an outlook will be given on promises and challenges in future developing of Pt transition metal alloy nanostructures towards fuel cells catalysis uses.

Keywords: low Pt nanocatalysts; transition metals; in situ characterization; electrocatalysis; oxygen reduction; methanol oxidation

1. Introduction

Polymer electrolyte membrane fuel cells (PEMFCs) have great application prospects in transportation, communication, military and space as an important renewable energy source for their high efficiency and low environmental impact [1,2]. Among various types of PEMFCs, direct methanol fuel cells (DMFCs) are considered to be a promising technology for efficient power sources in transportation and portable electrical devices due to their numerous advantages, including high power density and reliability. The efficiency of DMFCs is mainly limited by the sluggishness of electrode reactions. To facilitate the practical use of fuel cells, active electrode catalysts are necessary. So far, platinum (Pt) is the best catalyst for both the cathode with oxygen reduction reaction (ORR) and anode with methanol oxidation reaction (MOR). However, the scarcity and expensiveness of Pt have always hindered the further spread of fuel cells. Therefore, an investigation in reducing the amount of Pt use without compromising high activity and durability of electrocatalysts is highly desirable. A commonly applied approach is to alloy Pt with 3d transition metals (M, where M = Fe, Co, Ni, Cu, etc.), which even leads to substantial enhancement in electrocatalytic performance [3–8]. Essentially, this enhancement in performance can be ascribed to synergic effects, with which extensive investigations have been conducted on fathoming the correlation between nanostructures and enhanced catalytic performances. For instance, lattice strain has been acknowledged to be pivotal in core@shell catalysts,

a structure that promotes catalytic activity and durability by large margin. Density functional theory (DFT) calculations have confirmed that strained Pt shell has modified d-band structure and thus has lower absorption energy of oxygen species [9]. As a result, activity improves as the major hindrance of both ORR and MOR is decimated. Likewise, the surface transition metal composition induced ligand effect was found to greatly improve activity as well. As evidenced by in situ X-ray absorption spectroscopy, introduction of Nb suppresses the adsorption of oxygen species on Pt, thus led to a similar function as in strain effect [10]. In a more general concern, the exterior morphologies of the catalytic materials are the determining factors for the atomic configuration and electron structure of the catalyst surfaces, which directly affect the electrochemical adsorption of the reactant molecules and their decomposition. Therefore, the design and synthesis of multicomponent low-Pt nanocatalysts have attracted extensive research attention. Numerous studies on maneuvering shape, composition, and structure architecture have been reported. Well-defined Pt-based polyhedral nanoparticles (NPs) have been synthesized through varied approaches, such as octahedra [11], tetrahedra [12], icosahedra [13], and excavated or concaved polyhedral [14,15]. Also, various Pt-based nanoalloy exterior structure architectures, such as hollow nanoshells [16–18], nanobowls [19,20], nanochains [21,22], nanowires [23], nanomultipods [24,25], and hierarchical structures [26,27], have been fabricated in carefully designed manners.

For years, the threads in design of Pt alloyed nanocatalysts have been fixated on the molecule level chemical pathways of electrochemical reactions and have received desirable results [28,29]. The precise forecast on the exact effects structure takes on performance, however, is too complex to be theorized and is still wanting. Thankfully, owing to the rapid development of (in situ) characterization techniques, such as (in situ) X-ray absorption fine structure (XAFS) and (in situ) electron microscopy (EM), a new starting point is offered to us to investigate structure-performance correlation through (in situ) structural characterization. Devoted to monitor the structural evolution of nanocatalysts during synthesis and electrochemical process, researchers have unraveled several atomic origins of enhanced Pt-based nanocatalysts performances with concrete experimental evidences [30–32]. These techniques can offer the information about Pt alloyed nanocatalysts' microstructures, chemical compositions, and their dynamic behaviors, which enable us to establish the synthesis-characterization-performance relationships and further direct the design of new electrocatalysts with high performances.

This review will summarize the threads in design for Pt alloyed nanocatalysts derived from recent experiment and computation findings. Following these threads, structure designs and composition control will be summarized with their widely practiced synthetic approaches. Specifically, their key factors in effectively achieving shape- and composition-control will be underscored. Afterwards, commonly utilized methods along with several novel techniques in characterization will be introduced. The results in revealing structure-performance correlation with these characterization methods will be elucidated in coordination with the design threads. Then, recent progress in elevating the activity and durability for both ORR and MOR are presented along with their structure-performance correlation clarified. Several studies on bifunctional catalysts will also be introduced. Lastly, perspectives will be put forth regarding the difficulties and future direction in promoting Pt alloyed catalytic performance.

2. Design and Synthesis for Pt Alloyed Nanostructures

2.1. Design of Low Pt Alloyed Nanocatalyst with High Performance

It is generally recognized that the catalytic performance is mainly determined by the surface or the near-surface region of the catalyst. Engineering the surface properties, including the surface electronic structure and atomic arrangement of the catalysts, is believed to effectively tune catalytic properties of Pt-based catalyst, enabling enhancement in both the activity and durability of catalyst. Recent studies that revealed several effects various structures take on catalytic activity and durability provide many insights in designing high active and durable electrocatalysts. Investigation on NiPt NPs suggested that moderate annealing (at 300 °C) will enhance the binding of adsorbed surface

species as compared to unannealed and overly annealed (at 500 °C) samples, which boosts its activity towards ORR [33]. Moderate annealed NiPt NPs experience pronounced surface faceting and Ni atoms dissolution, which impairs its durability. That is, compromise in terms of durability has to be made to promote activity. Similar competing trends have also been observed for Pt-based nanocatalysts alloyed with other transition metals [34]. In addition, study on MPt (M = Co, Ni, Cu) nanoalloys indicated a linear correlation between ORR activity and Pt–Pt bond length where the ORR activity elevates with the reduction of Pt–Pt distance, a reduction that can be realized by tuning composition ratio or constructing hollow structures [30]. Another recent study suggested the significant role that M (M = 3d transition metal) content plays in electrocatalytic durability, where the removal of sub-surface M during electrochemical tests strengthens the Pt–O bond [35]. Keeping M content excessive is pivotal in terms of durability, such that specific activity would move towards the apex in Sabatier’s volcano plots as Pt–O bond strengthens during electrochemical process (Figure 1). Follow this thought, however, the relation between Pt–Pt bond length and specific activity appeared a volcano shape in this work, in contrast with the linear relation mentioned earlier. It hints that structural factors can modify the pattern that M content solely takes on activity.

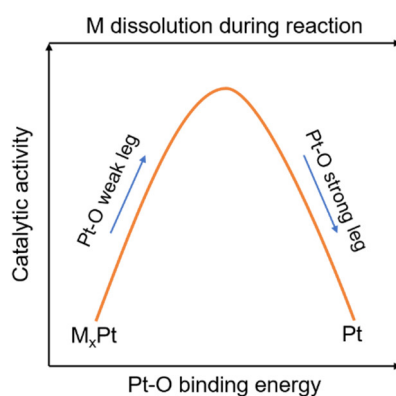


Figure 1. Illustration of catalytic activity of MPt catalysts as Sabatier volcano-type function of Pt–O binding energy [35]. An optimal design of Pt-based catalysts should let Pt–O binding energy place at the weak leg near the apex in order to balance the competition between activity and durability.

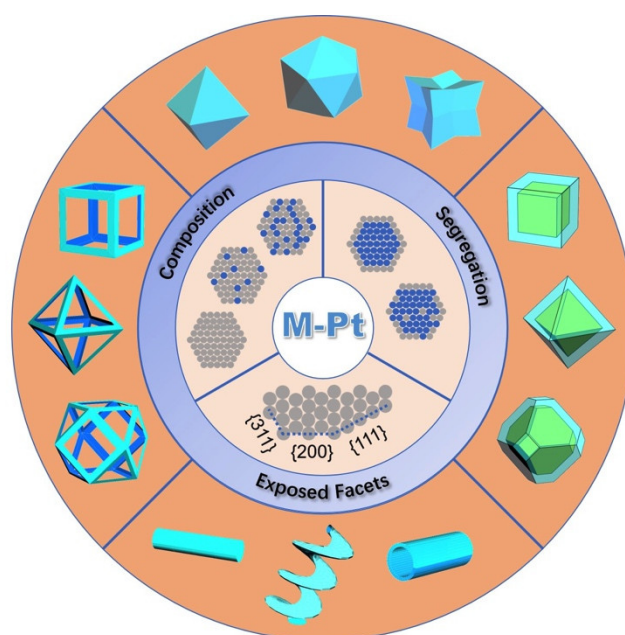
Among various structural factors, composition segregation, namely, core@shell or Pt-skin structure, has the most pronounced impact on performance. As ligand effect is blocked by Pt skin layers, strain takes on the most influence in core@shell structure. The compressive strain would modify the d-band structure, alleviating the intermediates absorption, as confirmed by DFT calculations [9]. In situ observation on CoPt/C NPs indicated a linear dependence of specific activity on strain induced by core@shell structures [36]. This linear dependence agrees well with the aforementioned relation between activity and Pt–Pt bond length. In addition, the Pt-skin layer can protect core part contents, since dissolution of Pt is much mitigated than that of transitional metals [37].

Another important structural factor is exposed active surface. For a catalyst, the variation of surface structure greatly affects its catalytic activity. Studies of single crystal Pt electrodes revealed that the catalytic activity varies at different crystal facets. In HClO₄ electrolytes, for instance, the order of activity for ORR is Pt(111) > Pt(110) > Pt(100) [38]. Meanwhile, high-index facets of face-centered-cubic (fcc) metals, as compared to stable low-index planes, generally exhibit significantly enhanced catalytic activity. That is because high-index facets have higher density of atomic steps, ledges, and kinks. Microstructure characterization on Pt NPs revealed a positive correlation between MOR activity and fraction of high-index facets, where higher activity was obtained when more surface steps were formed, leading to a higher percentage of high-index facets [39]. Same trend has been observed in Pt catalysts towards ORR [40]. Accordingly, selective exposure of different indexed facets is to be held crucial.

Hitherto, the threads for designing high performance low-Pt alloyed nanocatalyst can be summarized as follow:

1. the kernel of design is to balance the competition between activity and durability;
2. moderate transition metal M content is crucial such that the resulting Pt–O binding strength falls over the region in volcano plot with both high activity and durability; and,
3. structural design that brings about composition segregation as well as selective facets exposure with high fractions of electrochemically favored and/or high-index facets provides additional activity boost into pre-balanced activity and durability.

Bearing these threads in mind, performance of low-Pt alloyed nanocatalysts can be effectively tuned through composition and structure design (Scheme 1). To fully exploit the roles M content, Pt-enriched segregation, and exposed facets play in promoting performance, four types of structure designs are developed in addition to composition control. As illustrated in the outer ring in Scheme 1, they are polyhedra, hollow/frame structures, core@shell structures, and anisotropic structures. Next, we will take a tour into an in-depth discussion over the aspects in the design mentioned above.



Scheme 1. Schematic illustration of three key factors (inner/mid ring) in Pt alloyed nanocatalysts design, along with four types of structure architecture (outer ring) that partially or fully actualize these factors. Gray atoms in the inner ring represent Pt, and blue atoms represent M.

2.2. Structure Design

2.2.1. Alloy Polyhedra

Alloy catalysts with a lower content of expensive Pt metal can not only inherit the properties of the Pt constituent, but also usually show a superior performance when compared with monometallic Pt. The catalytic enhancement induced by synergy effects is evidence that, when comparing to Pt monometallic NPs, bimetallic or multimetallic Pt-based NPs with the same type of polyhedron displayed better ORR performance [41]. The origin of alloy polyhedral design is on the exposed facets, which are typically low-index and within different ratios. Pt {111} facets have been known to exhibit the highest activity, however, electrochemical process is rather intricate to favor this one-directional trend. On one hand, icosahedra do indeed show higher activity than octahedra, with their enclosed {111} facets being higher in quantity than octahedra [42]. On the other hand, truncated octahedra displayed a superior activity when comparing to octahedra, despite the truncated surfaces lowering the {111} to {100} ratio [43]. Nevertheless, the polyhedral exposed facets configuration is still pivotal in low-Pt alloyed nanocatalysts design.

Typical synthetic approach towards Pt alloyed polyhedra is solvothermal, a wet-chemical co-reduction method that is mostly favored for its simple, facile, and portable nature. One particularly facile solvothermal approach is Oleylamine (OAm) reduction [44]. Monodispersed Pt_3M ($M = Co, Fe, \text{ and } Ni$) nanocubes (NCBs) can be easily obtained with OAm reduction, where platinum(II) acetylacetonate $[Pt(acac)_2]$ and M -salt are co-reduced in a mixed solvent of oleic acid (OAc) and OAm carried out at around $240\text{ }^\circ\text{C}$ [45]. Octahedra Pt alloyed NPs, however, is not as easy to obtain, for its enclosed surfaces, $\{111\}$ facets, are more inclined to vanish during synthesis because growth on facets with low surface energy is faster compared to that on those with higher surface energy. To solve this conundrum, capping agents are employed in surface controlling solvothermal synthesis. In an OAm reduction that obtained NiPt octahedra with high ORR activity [46], Pt and Ni precursors were $Pt(acac)_2$ and $Ni(acac)_2$, respectively, while $W(CO)_6$ were added, which provided CO as capping agent towards Pt $\{111\}$ facet and led to the formation octahedral shape. Other effective surfactant or solvent with capping ability includes dimethylformamide (DMF) [47], polyvinyl(2-pyrrolidone) (PVP) [48], and benzyl ether (BE) [49]. Through this facile co-reduction method with capping agent additives, cubes with six $\{100\}$ facets [49], octahedra with eight $\{111\}$ facets [46], truncated octahedra with six $\{100\}$ facets and eight $\{111\}$ facets [50], and icosahedra with 20 $\{111\}$ facets [51] have been synthesized and measured to have superior catalytic activity (Figure 2a–d).

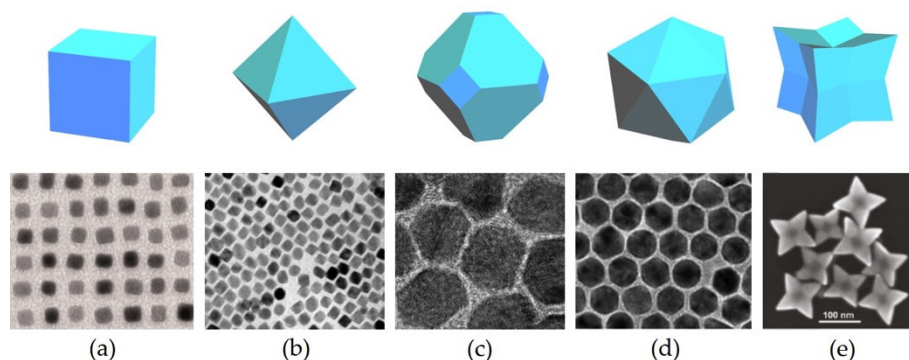


Figure 2. Illustrative models of (a) cubes; (b) octahedral; (c) truncated octahedral; (d) icosahedra; and (e) concaved polyhedra and their representative transmission electron microscopy (TEM) or scanning electron microscopy (SEM) images. The TEM image in (a) was reprinted with permission from reference [49]. Copyright 2012 American Chemical Society. The TEM image in (b) was reprinted with permission from reference [46]. Copyright 2013 American Chemical Society. The TEM image in (c) was reprinted with permission from reference [50]. Copyright 2016 American Chemical Society. The TEM image in (d) was reprinted with permission from reference [51]. Copyright 2012 American Chemical Society. The SEM image in (e) was reprinted with permission from reference [15]. Copyright 2011 American Chemical Society.

In addition to polyhedral enclosed with low-index facets, concaved or excavated structure with high-index facets exposed also showed exceptional enhancement in catalytic performances, although the origin for correlation between high-index facets and elevated performance is still unclear. To create a concaved or excavated structure, additional surface regulator, such as methylamine [15], cetyltrimethylammonium bromide (CTAB) [52], and cetyltrimethylammonium chloride (CTAC) [14], should be included in solvothermal synthesis. Note that synthesis condition and the amount of surface regulator have substantial impact on the final morphology. For example, in a synthesis system where glycine serves as the key of shape-control of CuPt NPs [53], with increasing glycine from 15 to 30, and then to 60 mg, concaved nanocubes, excavated nanocubes, and tripods (overgrowth) are formed. The carefully tailored synthesis protocol is therefore crucial. Differences in amount, reaction temperature, or time may lead to hollow structures, which is not undesirable and sometimes results in extraordinary performance enhancement as compared to solid Pt alloyed polyhedra.

2.2.2. Hollow and Frame Structures

The advantage of hollow structure includes, but is not limited to, increased specific surface area, more low coordination surface steps, and electrochemically robustness. The frame structure gives greater play to these advantages. In exploiting the Kirkendall effect, where vacancy defects form as a consequence of diffusion among metal atoms with varied diffusion rates, hollow structures can be formed from template-removal. Xia et al. [54] reported a one-pot synthesis of CuPt cubic nanocage with Cu and Pt precursors dissolved in CTAB and OAm and solvothermally treated. The appropriate amount of CTAB was thought to be essential for hollow nanocage formation, in consistency with the concaved polyhedral structure formation discussed above. Later, Chen and Kang et al. [55] proposed a nanoframe synthesis that exploited NPs evolution (Figure 3a), in which Ni₃Pt octahedra were further thermally treated in nonpolar solvents such as hexane and chloroform to form NiPt₃ nanoframes. Essentially, the formation of nanoframe relies on the dissolution of transition metal. Therefore, the product morphology depends on both the template shape and transition metal composition. Stamenkovic and Yang et al. [56] recently demonstrated precise control over three-dimensional (3-D) morphology of NiPt nanoframes in OAm reduction scheme followed by Ni corrosion through tuning the concentration and ratio of Pt and Ni precursors (Figure 3b). Conventional hollow nanoframes were obtained with high Ni concentration, while excavated nanoframe with low Ni concentration. In another study, a set of NiPt nanoframes were synthesized by a simple OAm/OAc co-reduction approach followed by acetic acid leaching [57]. Morphology variation from tetrahedral to rhombic dodecahedral template was achieved in by altering the OAm to OAc ratio thus result in nanoframes with different morphologies (Figure 3c). As open hollow structure provides large specific surface area and possibly high fractions of high-index facets, as-synthesized nanoframes typically possess composition segregation, namely, Pt-rich surface layers, that further contributes to catalytic performance in terms of durability.

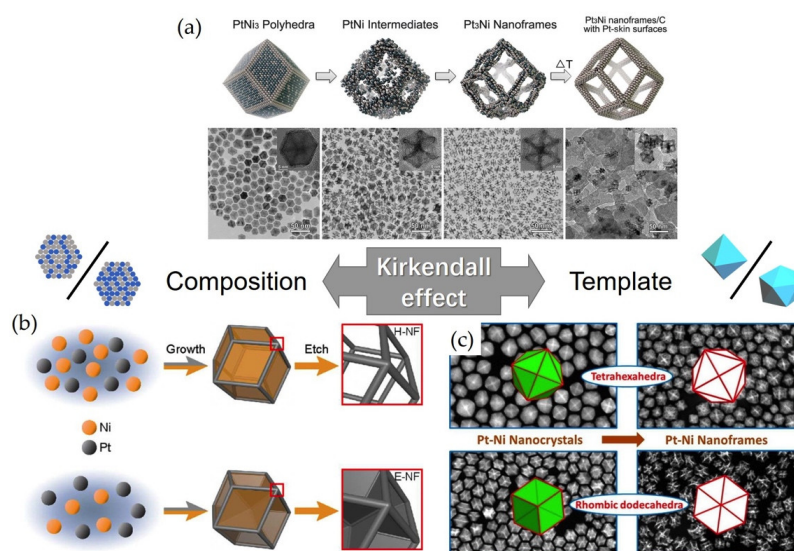


Figure 3. Evolution process from polyhedra to nanoframes exploit Kirkendall effect. Two key factors determine the final morphology in exploiting Kirkendall effect: composition and template. (a) Schematic illustrations of the Ni_xPt_{1-x} samples obtained at four representative stages and their corresponding TEM images. From reference [55]. Reprinted with permission from American Association for the Advancement of Science (AAAS); (b) Schematic illustrations of the synthetic routes to fabricate i. hollow nanoframe (H-NF) and ii. excavated nanoframe (E-NF) with different metal precursor ratios. Reprinted with permission from reference [56]. Copyright 2017 American Chemical Society; (c) Schematic illustrations of NiPt polyhedra and their outgrowth nanoframes with different morphologies and their corresponding TEM images. Reprinted with permission from reference [57]. Copyright 2016 American Chemical Society.

2.2.3. Pt-Skin

Pt alloyed nanocatalysts commonly show exceptional performance possessing surfaces-exposed Pt-skin or Pt-rich layers. Since the dissolution of Pt is much more mitigated than that of transition metals, Pt-skin, or core@shell structure, display much enhanced long-term durability comparing to unsegregated nanocatalysts [37]. To fabricate a Pt-enriched surface, post-treatments, such as electrochemical and chemical and chemical dealloying, are usually applied on as-prepared unsegregated seeds [58–60].

In concerns of activity, however, the surface modification derived from the underlying transition metals occurs only when Pt surface layer is thin enough. DFT results show that a Ni atom can affect significantly the d-orbitals electronic distribution of its nearest and sub-nearest neighbor platinum, while the intrinsic activity of such catalysts drops and approaches to that of pure Pt with increasing skin thickness [61]. Therefore, precise controlling of the Pt-skin thickness is pivotal. To achieve that, electrochemical underpotential deposition (UPD) can be used to construct well-defined layers of transition metal M on as-prepared seeds (Figure 4a). In this case, UPD is commonly coupled with galvanic replacement of M by Pt atoms in order to form a Pt surface layer. Ghosh et al. [62] utilized UPD, followed by galvanic replacement in synthesizing Pt monolayer on intermetallic MPt NPs. In this sense, Pt-skin with any number of layers can be fashioned through layer-by-layer deposition of Pt monolayers onto as-prepared seeds (Figure 4b,c) [63]. In a second approach, Pt precursors directly react with as-synthesized seeds through UPD. Under this case, the resulting Pt shell thickness is usually not well defined [64].

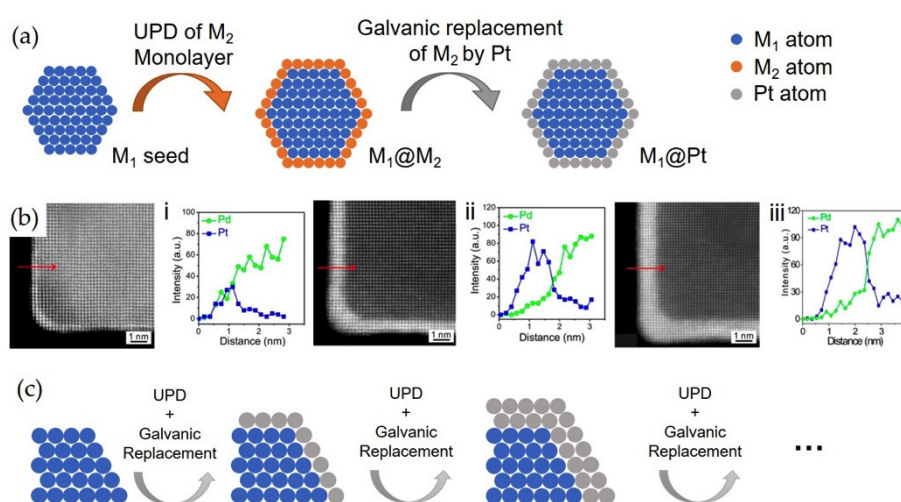


Figure 4. (a) Schematic illustration of underpotential deposition (UPD) coupled with galvanic replacement to fashion a well-defined Pt monolayer skin; (b) High angle annular dark field scanning transmission electron microscopy (HAADF-STEM) images and the energy dispersive X-ray spectroscopy (EDS) line scan along the red arrows taken from the Pd@Pt nanocubes with i. one Pt atom layer, ii. four Pt atom layers, and iii. six Pt atom layers. Reprinted with permission from reference [63]. Copyright 2014 American Chemical Society; (c) Schematic illustration of fabrication of Pt-skin with any number of layers.

2.2.4. Anisotropies

Anisotropic nanostructures, such as nanowires [23], nanochains [65], nanorods [66], and nanodendrites [67], as compared with zero-dimensional (0-D) nanocatalysts, have several advantages in terms of both activity and durability. Anisotropic nanostructures usually exhibit high catalytic performance due to their high surface area and exposed high-index facets resulting from the highly reactive edges, corners, and stepped atoms on their surfaces. Furthermore, Pt-based 0-D nanocatalysts are usually supported on the high surface area carbon blacks, which are easily corroded under

electrochemical condition. However, comparing to the 0-D Pt nanoparticles, anisotropic nanostructures are more stable, because they tend not to easily dissolve, migrate, Ostwald ripen, or aggregate. Similar to those in concaved and hollow structure, additives serving as structure-directing agent are crucial in anisotropic structure formation. In a solvothermal preparation of hierarchical CoPt nanowires, the amount of CTAC was found to be pivotal in forming exposed high-density high-index facets (Figure 5a) [26]. Also, the introduction of Co precursor was determinative in the work, as the hierarchical nanowires were formed from the intermediate pure Pt nanowire seeds after Co precursor was injected. Similarly, CuPt nanotubes were synthesized by a seed-mediated method with as-prepared Cu nanowire and the addition of Pt precursor [68].

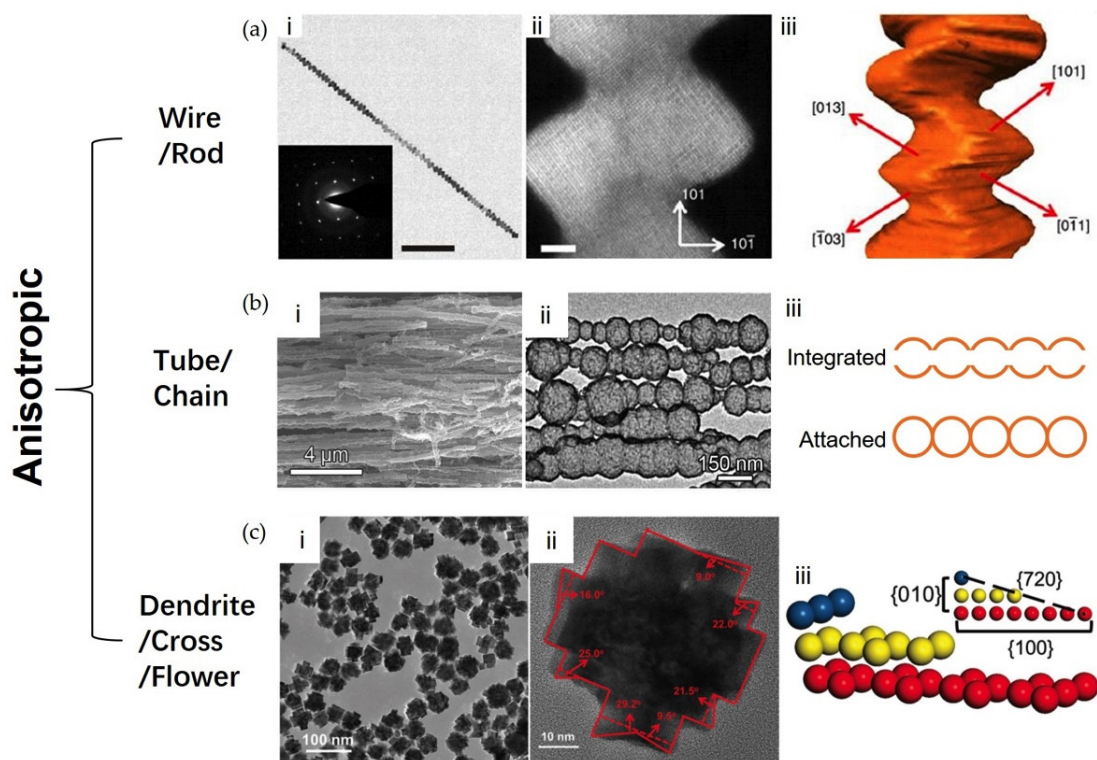


Figure 5. Three typical morphologies of anisotropic structure: wire/rod, tube/chain, and dendrite/cross/flower. (a) i. TEM and ii. HAADF-STEM images of hierarchical CoPt nanowires; iii. indexes of the exposed facets of CoPt nanowires; (b) SEM and TEM images for hollow FePt nanochains. Different synthetic route led to different types of nanochains; (c) i. TEM and ii. HRTEM image of crossed CoCuPt; iii. Atomic illustration of {720} facet associated with the angle 29.2° shown in ii. Images and model in (a) were reprinted with permission from reference [26]. Copyright 2016 Nature Publishing Group. Images in (b) were reprinted with permission from reference [21]. Copyright 2016 Royal Society of Chemistry. Images and model in (c) were reprinted with permission from reference [69]. Copyright 2018 John Wiley and Sons.

To fully exploit nanoscale assembly, other approaches have been utilized in fabricating complex anisotropic nanostructures. For instance, FePt nanochains that were obtained by our group (Figure 5b) [21] were assembled, template-free, from hollow FePt nanospheres that were prepared through a wet-chemical synthesis in room temperature. The as-prepared hollow FePt nanospheres were then applied with external magnetic field while continuously adding Pt precursors. External magnetic fields changed the motion of atoms, molecules, and ions during the chemical reactions, which helped to align the nanoscale assembly thus formed the chain shape. Note that the time of addition of Pt precursor is crucial for the product morphology, and hence, the performance. Injecting Pt precursor at two stages of the magnetic-assisted growth results in either integrated or attached nanochains

(Figure 5b). Aside from one-dimensional wires or tubes, for ternary alloy nanocatalysts, characteristic crossed structures that exhibit large surface area with exposed high-index facets (Figure 5c) can be easily fabricated through chemically induced self-assembly [69,70].

2.3. Composition Control

As suggested before, the M content should be moderate to balance the competition between activity and durability. However, variety in elements and morphologies alter the volcano-type relation between activity and Pt–O bond length, and, accordingly, M to Pt ratio. Since no directory formula is investigated for each structure with each transition metal, along with the needs to balance performance between Pt usage, works on Pt alloyed nanocatalysts usually carried out with a set of samples with different composition. In solvothermal synthesis, control over the molecular ratio is quite straight forward, where the metal-to-metal ratio in precursors determines the products composition. Other factors such as reaction temperature and duration could also affect overall composition. For instance, in a preparation of NiPt NPs, the reaction was held at 120 °C, while the near-surface composition was controlled, without affecting the NPs' sizes or shapes, by varying reaction time, i.e., the near-surface Pt at. % increased from 30 to ~41 at. % when the reaction time was raised from 16 to 42 h [47].

A more important practice in manipulating the composition is composition segregation, especially on the surface and sub-surface part of nanostructures, for surface and sub-surface composition influences surface strain, which prominently affects electrocatalytic performance [71,72]. As discussed before, dealloying is an effective tool in altering the surface composition. The initial composition of the as-prepare seeds has a significant impact on the composition, in both surface and sub-surface, of dealloyed NPs. Gan et al. [73] discovered a notable Ni-rich inner shell formed near the surface of dealloyed Ni₃Pt NPs, but not as such in NiPt NPs (some address this as Pt sandwich segregation structure) (Figure 6). This Ni-rich inner shell led to a higher extent of compressive strain, which resulted in elevated catalytic activity.

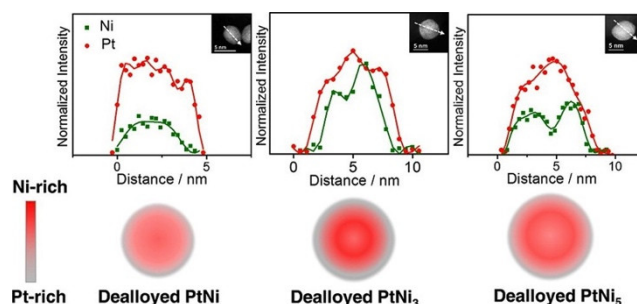


Figure 6. Composition distributions of dealloyed NiPt nanoparticles (NPs) with different initial atomic ratios and their corresponding electron energy loss spectroscopy (EELS) line profiles. Reprinted with permission from reference [73]. Copyright 2014 American Chemical Society.

Besides strain effects, surface or subsurface transition metal induced ligand effect also plays a crucial role in promoting catalytic performance [74]. Under this consideration, annealing provides more flexibility in tuning activity and durability, as it takes a bidirectional effect on (surface) composition segregation. Conventionally, atomic reordering by annealing was thought to mainly take effect in converting disorder phase into ordered one. Recent findings suggest an invert course, where annealing process in certain oxidizing and reducing atmospheres, such as CO, NO, O₂, and H₂, can lead to reverse reconstruction of phase and composition, addressed in some literatures as adsorbate-induced segregation [64]. In this case, either Pt preferentially segregates over the transition metal M, forming a Pt-rich surface [75], or the other way around [76]. Zhang et al. [77] recently demonstrated surface composition-control over CoPt NPs via adjusting the annealing atmosphere. They obtained intermetallic phase under argon atmosphere at 700 °C, whereas Co-rich under air at 300 °C and Pt-rich under 10% H₂/N₂ at 700 °C (Figure 7). As the strain effect and ligand effect

occur concurrently, a comparative study on their exclusive roles can be more intensively studied via annealing post-treatment.

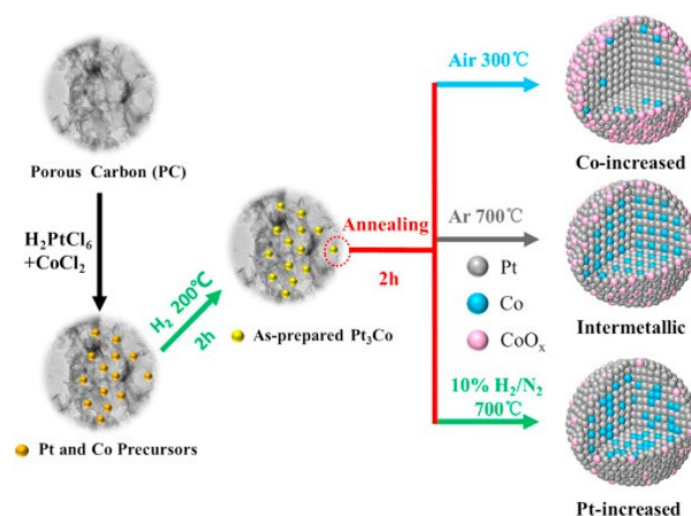


Figure 7. Schematic illustration of fabricating Pt₃Co/PC catalysts and tuning their surface composition via adsorbate-driven segregation at different annealing atmospheres. Reprinted with permission from reference [77]. Copyright 2017 Elsevier.

3. Microstructure Characterization

In need of optimizing catalysts performance, researchers have devoted to search for correlation between microstructures of low-Pt alloyed nanocatalysts and their mesoscopic characteristics, and even to fathom the functional links between them. Such microstructural measures involve geometry, composition, surface, and interface. Owing to the advanced development in electronic microscopy (EM), diffraction, and energy spectroscopy, the ex situ characterization of nanocatalysts has becoming comprehensive and exhaustive. However, the needs still existed to monitor structure evolution in NPs synthesis and behaviors in electrochemical environment. To gain further insight on the structure-performance correlation, in situ characterization on atomic arrangement and electronic structure etc. is becoming essential. In this section, we will discuss the microstructure characterization progress for Pt alloyed nanocatalysts and elucidate their result in understanding the origin of catalytic performance.

3.1. Electron Probing

Typical electron probing techniques in nanostructure characterization involve scanning electron microscopy (SEM) and transmission electron microscopy (TEM). Sampling the reflected or transmitted electrons, SEM and (high resolution, HR-) TEM are commonly utilized in confirming exterior morphology and imaging the lattice structures with sub-atom resolution. Meanwhile, high angle annular dark field scanning transmission electron microscopy (HAADF-STEM) can give further insight in 3D morphology and element composition, for it employs Z-contrast imaging [78].

In order to monitor dynamic evolution of nanocatalysts especially their degradation during electrochemical process, several advanced EM approaches have been developed. Identical-location TEM (IL-TEM, ex situ) has been successfully utilized in revealing the degradation mechanism of electrocatalysts [79]. In IL-TEM, a specially made TEM sample holder (typically a gold grid), was used as a support that allows the electrocatalysts sample to take electrochemical tests and TEM imaging in turns. Though inspiring results have been received, the process is inefficient in nature. Thanks to the progress of in situ EM, the tracing of structure evolution for nanocatalysts in fabrication or activation has become more direct. Time-resolved TEM images of as-prepared NiPt NPs showed the morphology changes during annealing at escalating temperatures in inert conditions (Figure 8) [80]. Flat {111}

surfaces of the cuboctahedra were determined to be stable over a wide temperature range. In a similar study, the formation of NiPt NPs were determined to be highly dependent on treatment temperature, where incorporation of Ni-rich alloys (formed at a moderate temperature) into octahedra particles (formed before annealing) happened only at a higher temperature [33]. These results provide synthetic possibilities for promoting catalytic performance through tailoring activity-durability relationship of octahedral NPs.

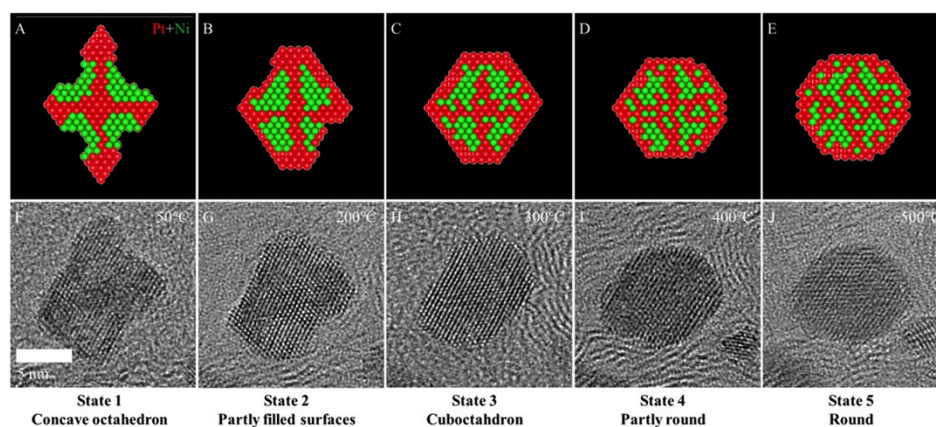


Figure 8. Illustrations (a–e) of proposed Pt (red) and Ni (green) atomic distributions in NiPt octahedra that undergo transformations during in situ thermal heating at escalating temperature and their corresponding HRTEM images (f–j). Reprinted with permission from reference [80]. Copyright 2018 American Chemical Society.

Formation mechanism of anisotropic Pt-based catalysts can also be observed through in situ TEM. Using a gas cell holder, Ma et al. [81] were able to study the growth process of Pt nanowires in H₂ (Figure 9). First, the growth of small NPs was observed after nucleation. Later, oriented attachment occurred through rotation and particle movement assisted by H₂, for Pt surface was modified by preferential coverage of H₂. This result illustrates the role that gas plays in metal surface diffusion in catalysts fabrication, which leads to a direction towards which anisotropic Pt-based catalysts synthesis can be designed.

Nevertheless, when compared to time-resolved formation observation in nanocatalysts synthesis, only a few reports have employed in situ (environmental) EM in electrochemical process [82–84]. The irradiation of electron beam is the main issue that sets the limit of electrochemical in situ EM, for it can cause water radiolysis, lowering of electrochemical potential, and disruption in electric field that induces difficulty in controlling the electrochemical potential of the sample [85]. Therefore, works still need to be done for the competent application of in situ EM towards nanocatalysts characterization.

Another point of notice in electron probing is electron energy loss spectroscopy (EELS). EELS is typically coupled with TEM/STEM to gain further insight regarding composition distribution. When comparing to another element mapping technique i.e., energy dispersive X-ray spectroscopy (EDS), however, EELS presents some drawback regarding accessibility in terms of hardware and operation, and, accordingly, EDS has been more popularly employed in element mapping. Nonetheless, EELS mapping has its own edge in higher efficiency and higher energy resolution. Also, energy loss near edge structure (ELNES) can be used to study electronic structure and valence state, which can give additional insight into chemical process [86]. Therefore, with the promising development in microscopy techniques and instruments, EELS can be applied more favorably in characterization for alloy nanocatalysts.

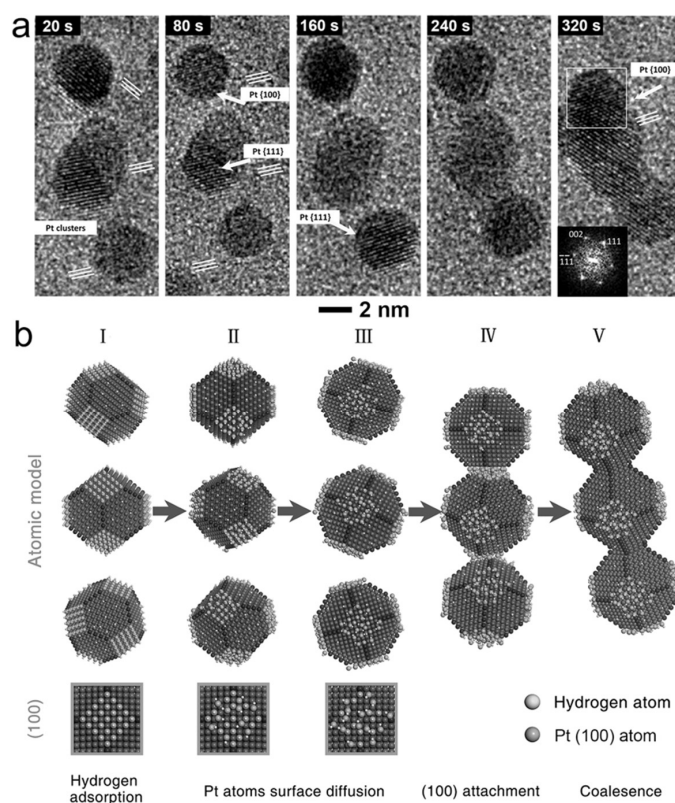


Figure 9. Illustrations of oriented attachment in Pt nanowire formation and corresponding atomic model. The parallel white lines in (a) indicate the lattice orientation before and during attachment. Schematic illustrations in (b) shows the early connection stage, including hydrogen adsorption, Pt-atoms surface diffusion enhanced by CO, oriented attachment at Pt {100} facets, and finally coalescence to short chain. Reprinted with permission from reference [81]. Copyright 2017 John Wiley and Sons.

3.2. X-Ray And Infrared Probing

X-ray spectroscopy is conventionally employed in evaluating electron structures in Pt alloyed nanocatalysts. Two types of X-ray spectroscopy are commonly applied: X-ray photoelectron spectroscopy (XPS) and X-ray absorption spectroscopy (XAS). In a general sense, XPS provides information of atoms valence state and chemical bonds in nanocatalysts through measuring the binding energy of inner shell electrons and their chemical shifts. On the other hand, exploiting electron excitation between atomic energy bands puts XAS in advantage, for it provides insight into finer electron structure. X-ray absorption fine structure (XAFS) is typically utilized in characterizing fine electron structure in Pt alloyed catalysts. XAFS includes X-ray absorption near edge structure (XANES) and extended X-ray absorption fine structure (EXAFS). The interference between excited photoelectrons and scatter photoelectrons depends the atomic band structures, coordination numbers, and atomic bond length, and therefore can provide information of short-range structures. In situ XANES characterization on octahedral NiPt/C of Pt L_3 -edge evidenced a modification in electronic structures of core Pt atoms induced by neighboring Ni atoms [32]. Meanwhile, in situ EXAFS showed a weak absorption of oxygenated species (weakened Pt–O bond) in the same work, revealing atomic origin for enhanced catalytic performance.

Moreover, surface atomic structure model of nanocatalysts can be deduced with the information gathered from XAFS. In situ XANES of Ni K-edge and Pt L_3 -edge performed on NiPt/C nanoframes catalysts before and after the electrochemical process indicated a surface with more low-coordination sites and thinner platinum shell in one particular sample, for Ni is more easily oxidized in this sample, as evidenced by more intense peak in the XANES difference spectrum, as shown in Figure 10 [87].

Parameter fitting on further in situ EXAFS analysis determined the coordinate numbers and bond lengths, which subsequently yielded the composition ratio between Ni and Pt.

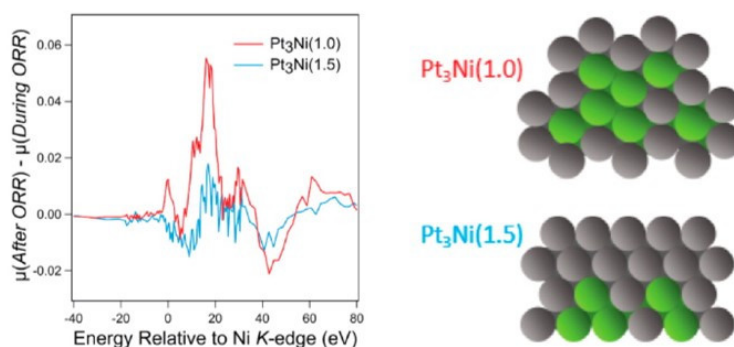


Figure 10. In situ Ni K-edge X-ray absorption near edge structure (XANES) subtracted from ex situ XANES after electrochemical process of NiPt/C nanoframes. On the right shows deduced surface atomic models of two as-prepared samples, where gray atoms are Pt and green atoms are Ni. Refer sample notation to original paper. Reprinted with permission from reference [87]. Copyright 2015 American Chemical Society.

These results, along with the preceding ex situ XANES, helped to rationalize the atomic model of the edge of NiPt/C nanoframes and its evolution during electrochemical process. Owing to its effectiveness in investigating short-range structures and the full-blown commercialized analytic hardware and software, XAFS is the foremost technique in electron structure characterization of Pt alloyed nanocatalysts.

Other than X-ray spectroscopy, infrared (IR) spectroscopy has also been utilized in revealing atomic or electron structures sometimes [31,33,88]. In situ IR spectroscopy has been proven handy in measuring surface atom configuration. Coupled with DFT calculation and in situ STEM analysis, in situ IR spectroscopy was applied to provide complementary sample-averaged quantitative information of CO-induced Pt NPs surface reconstruction [89]. The CO adsorbate on under-coordinated (UC) and well-coordinated (WC) Pt sites were differentiated by vibrational frequency dependency on charge transfer, where CO bonded to UC Pt sites has a larger amount of charge transfer thus resulted in a red shift. The obtained fractions of UC and WC Pt site provide insights in selective surface reconstruction of {100} facets. It is noteworthy that, despite that IR or X-ray cannot be converged, the sample-averaged information that resulted could evidence the universality of the particle-scaled TEM/STEM results.

4. Progress in Electrocatalytic Performances

Previous discussion on the design and synthesis of Pt alloyed nanocatalysts have provided threads for high electrochemical performance design and demonstrated several effective syntheses in shape-/composition-control and structure architecture following these threads. Further, characterization methods help to direct and revise these designs by unraveling the structure-performance correlation in order to obtain higher catalytic performance. In this section, we will discuss the catalytic application of Pt transition metal alloy nanocatalysts in ORR, MOR, and as bifunctional catalysts. The recent progress in light of the aforementioned threads will be highlighted.

4.1. ORR

Early researches on Pt-based transitional metal alloy nanocatalysts for ORR have concentrated on promoting activity by moderated binding between Pt atoms and intermediate oxygen species through tuning d-band center [90,91]. Ni and Co were determined to have the best enhancement towards ORR when comparing to other transition metals when alloyed with Pt [92]. Shape-wise, polyhedral morphologies once showed topnotch ORR catalytic performance, such as octahedra [46], truncated octahedra [43], and icosahedra [51]. The mainstream focus on Pt-based nanocatalysts towards ORR had

been continuously on NiPt, especially on structure with Pt₃Ni (111) surface, since it showed weakest oxygen binding energy [93]. In recent years, attentions in Pt transition metal alloy ORR catalysts have pivoted into structure design, since electrochemical endurance is gradually being regarded as paramount as activity in electrocatalysts developing. Zhao et al. [32] constructed carbon supported concaved octahedral core–shell PtNi with an exceptional ORR specific activity of 5.29 mA cm⁻² and mass activity of 1.69 A mg⁻¹. The mass activity suffered only a 3.7% loss after accelerated durability tests (ADTs) of 10 k cycles between 0.6 and 1.0 V. In situ XANES suggested a weakened oxygen species binding as compared to commercial Pt/C, while STEM-EDS analysis showed a compressive strain induced by core Ni content. Shortened Pt–Pt bond and the absence of strong Pt–O bond jointly promote its activity. The concaved surface Pt layer protects the core NiPt from dissolution. A more recent report of octahedral NiPt@Pt core@shell NPs also exhibited a high ORR specific activity of 3.66 mA cm⁻² and mass activity of 1.24 A mg⁻¹ [94]. Single cell tests on this catalyst suggested a great enhancement when comparing to commercial Pt/C in terms of both activity and durability of single cell operation.

Nanoframes and hollow structures have so far acted most prosperously in promoting both ORR activity and durability. 2D NiPt nanoframes fabricated by Godínez-Salomón et al. [95] showed an excellent ORR specific activity of 5.8 mA cm⁻² along with a high durability of only 6.9% specific activity loss after 1 k cycles of ADTs. The micropores formed within the nanoframe structures and segregation between surface and subsurface composition were thought to contribute to the enhancement in activity. The unsupported 3D structure and specific Pt atoms environment were believed to attribute to high durability. In another work, hollow FePt with Pt-skin that was synthesized by Wang et al. [96] showed high ORR specific and mass activity of 1.35 mA cm⁻² and 0.99 A mg⁻¹, respectively. Durability was also verified to be robust, due to the Pt-skin layer, with only 27% mass activity loss after 40 k cycles of ADTs. DFT calculation revealed the hollow structure with a Pt-skin can efficiently decrease the d-band center, hence the enhancement in activity. A comparison of the activity towards ORR of various MPt catalysts is shown in Figure 11. Other structures such as nanodendrites [67], nanoporous structures [97], nanobowls [20], and nanocages [98], have been reported to possess high ORR activity and durability as Pt transition metal nanoalloys in recent years. Most recently, complex frameworks, such as octopod nanoframes and multiframes. have displayed the highest performance [99,100]. Discussion on these types of structures will be covered in MOR section.

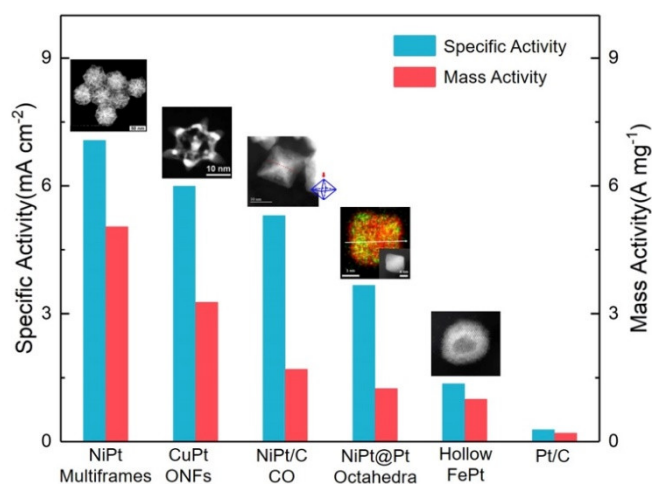


Figure 11. Comparison of various type of oxygen reduction reaction (ORR) Pt alloyed nanocatalysts that are reported in recent two years, including NiPt Multiframes [100], CuPt octopod nanoframes (ONFs) [99], NiPt/C concaved octahedra (CO) [32], NiPt@Pt octahedra [94], hollow FePt [96], and 20% Pt/C [96]. Inset images, from left to right were reprinted with permission from reference [32,94,96,99,100]. Copyright 2018 American Chemical Society, 2016 John Wiley and Sons, 2017 American Chemical Society, 2018 Elsevier, and 2016 John Wiley and Sons.

4.2. MOR

Similar to ORR, the major hindrance of MOR activity is the strong binding between Pt atoms and intermediate oxygen-containing carbon species (particularly CO) [101]. Alloying transition metal can relieve this problem, and the unique structural design can further boost the durability towards MOR environment [102]. Therefore, the track in MOR catalyst research have rather paralleled with that in ORR. Pt had been favored in Pt-based nanoalloy towards MOR catalysts [103,104]. More recently, reports on Pt transition metal nanocatalysts towards MOR with high activity and durability have emerged. Chronoamperometry (CA) showed enhanced durability when compared to commercial Pt/C. Truncated octahedral (TO) CoPt NPs that were synthesized by our group [105] and Cu@CuPt concaved octahedra (CO) obtained by Wang et al. [106] exhibit great enhancement in MOR performance, in great exploitation of facets and surface composition design.

Advanced structural design showed further progress in promoting MOR performance for Pt transition metal alloy nanocatalysts. Concaved CuPt octopod nanoframe prepared by Luo et al. [107] reached an exceptional MOR specific activity of 7.5 mA cm^{-2} and mass activity of 3.36 A mg^{-1} . 72% of initial current density was retained after 2 k cycles of ADTs. The extraordinary MOR performance was ascribed to synergy effects, exposed high-indexed facets and the framework structures. Comparison to ultrathin octopod nanoframes synthesized in the same work indicated that richer sub-surface Cu content also attributed to elevated activity, while the feet of concaved octopod nanoframes were proven to be more stable than the ultrathin edges thus strengthened durability. This provides a direction for designing nanoframes structures with higher performance. In another report, CuPt nanotubes obtained by Li et al. [68] showed an exceptional enhancement in MOR performance with a specific activity of 6.09 mA cm^{-2} and mass activity of 2.25 A mg^{-1} . In terms of durability, reactivation was achieved even after four rounds of 3000 s CA, with negligible activity loss. Surface strain that was observed was believed to help reconstruct an arrangement of surface Pt atoms, thus strengthening durability. A comparison of the activity towards ORR of various MPt catalysts is shown in Figure 12. Similar to ORR, frame structures display the highest performance towards MOR.

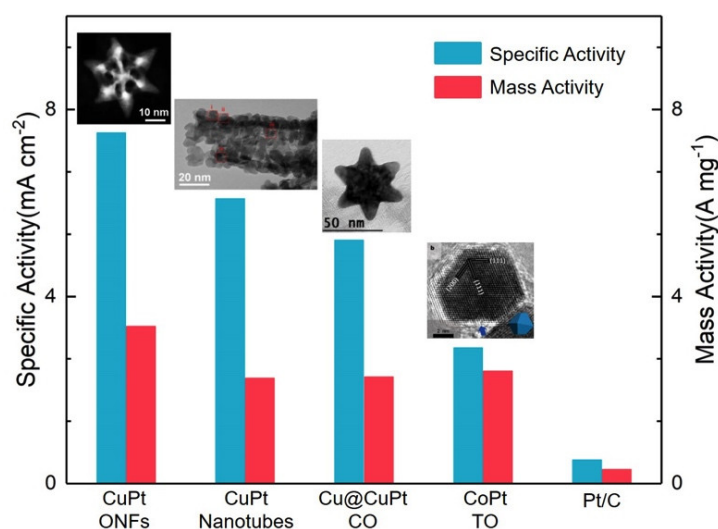


Figure 12. Comparison of various type of MOR Pt alloyed nanocatalysts that are reported in recent two years, including concaved CuPt ONFs [107], CuPt nanotubes [68], Cu@CuPt CO [106], CoPt TO [105], and 40% Pt/C [105]. Inset images, from left to right, were reprinted with permission from reference [68,105–107]. Copyright 2017 American Chemical Society, 2017 Royal Society of Chemistry, 2017 American Chemical Society, and 2016 Springer Nature.

4.3. Bifunctional Catalysts

In addition to the Pt alloyed nanostructures discussed above that showed significant boost in ORR or MOR catalytic performance, many works have reported active performance in both oxygen reduction and methanol oxidation reaction. These bifunctional catalysts will be of superior importance as they can function as active catalysts in both cathodes and anodes of DMFCs. Polyhedral NPs, such as octahedra [52,108], have evidenced applicability as bifunctional catalysts, as synergy effect can be fully implemented. For open structure, the nanoframe is always intriguing. Highly anisotropic five-fold-twined CuPt nanoframes that were synthesized by Zhang et al. [109] displayed great ORR and MOR activity with specific activity of 1.71 mA cm^{-2} for ORR and 18.2 mA cm^{-2} for MOR (Figure 13). The rich concaved sites with high-coordination numbers provided by five-fold-twin structures attribute to ORR activity. Twining defects modulate the electronic structures and surface reactivity, thus enhancing small molecule reaction, such as MOR. A very interesting point of notice in this work is the uncommon protruding nanothornes on the edge (Figure 13), for they provide extra active surface area and possibly high-index facets. Recently, Kwon et al. [110] fabricated Co-doped CuPt rhombic dodecahedral nanoframes that showed extraordinarily high MOR specific activity of 13.3 mA cm^{-2} and mass activity of 4.11 A mg^{-1} (Figure 13). ORR performance was also boosted with specific activity of 5.03 mA cm^{-2} and mass activity of 1.56 A mg^{-1} . A durability test suggested 86.1% of specific activity and 73.1% of mass activity for ORR, along with 63.5% of mass activity for MOR retained after ADTs with separate protocols (10 k cycles between 0.6 and 1.0 V for ORR, and 1 k cycles between 0.05 and 1.2 V for MOR). Interestingly, the protruding vertices play an irreplaceable role in boosting durability, as confirmed by comparative study with undoped CuPt nanoframes. These uncommon structures that either enlarge active surface area or reinforce the edges should be more extensively studied in the future. At last, nanowires [26] and other anisotropic structures have been discovered to be efficient in bifunction purpose. Also, Pt alloyed nanostructures have been reported to be active as bifunctional catalysts towards ORR on cathodes and other fuel oxidation reaction on anodes, such as ethanol [111], formic acid [112], and ethylene glycol [50].

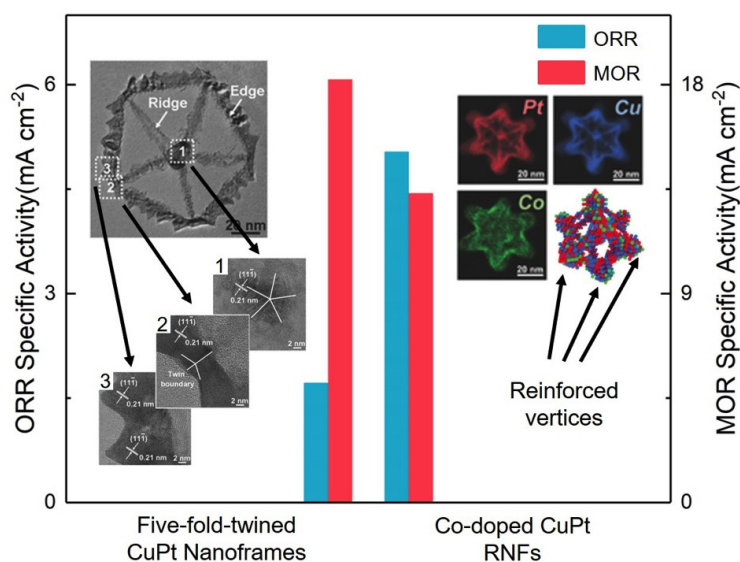


Figure 13. Comparison of two bifunctional Pt alloyed nanocatalysts: five-fold-twined CuPt nanoframes [109] and Co-doped CuPt rhombic dodecahedral nanoframes (RNFs) [110]. Inset on the left shows TEM image of five-fold-twined CuPt nanoframes with HRTEM images taken within dotted square 1, 2, and 3, which separately indicate five-fold twinning, twining boundary, and protruding structure. Inset on the right shows atomic model of Co-doped CuPt (RNFs) and EDS mapping of a single nanoframe. Note the reinforced vertices as marked by black arrows. Inset images on the left were reprinted with permission from reference [109]. Copyright 2016 John Wiley and Sons. Inset images on the right were reprinted with permission from reference [110]. Copyright 2018 John Wiley and Sons.

5. Summaries and Perspectives

In the efforts of lowering Pt usage in fuel cells electrocatalysts, Pt-transition metal alloy nanostructures have been proven to be an effective and favorable resort. In this review, threads that revolve around balancing the competition between catalytic activity and durability are first summarized. Synthetic approaches to fabricate and maneuver these catalysts that follow these threads are then introduced. Well-defined Pt alloyed polyhedra can be obtained through the solvothermal co-reduction approach, while carefully tailored dealloying, UPD, and annealing are underscored to gain further shape- and composition-control in hollow, framework, Pt-skin, and anisotropic structures. From these delicately designed structures and composition segregation, substantial enhancement in both catalytic activity and durability can be obtained. These structure-performance correlations were investigated through the (in situ) atomic and electronic structure characterizations, as discussed after. In situ EM and XAFS were highlighted for their effectiveness in characterizing nanostructures and alterations in surface electron structures. These findings, combined with the aforementioned design protocols, provide directory insights in promoting Pt alloyed nanocatalysts performance towards ORR and/or MOR, which were presented through discussion in recent reports.

Despite the numerous progress, many works still need to be done to further expand the use of Pt-transition metal alloy nanocatalysts. For instance, highly complexed structures that exhibit exceptional catalytic performances commonly cannot be obtained through a conventional one-pot synthesis. The prolonged duration and intricate procedure provide certain inconvenience, while the possible high-temperature treatment leaves a great inaccessibility in terms of instruments. Few alternatives have been raised, such as solution plasma sputtering [113], however, works remain to promote efficiency and yielding in concerns of practical uses. Another conundrum is the competition between activity and durability. Extra structural architecture on nanoframes is one effective way. As discussed above, reinforcing the vertices [110] and the edges [107] is a good direction for further strengthening structural robustness, while extra structure atop the frame edges [109] can provide extra active surface. Other ideas include modifying substrates with more robust structures [114–117], and introducing 4d or 5d transition metal that strengthens the ligand effect as well as its electrochemical durability [10,118]. At last, in light of Pt alloyed nanostructures' broadened application in magnetic or optical use [119], recycling used Pt alloyed nanocatalysts can be regarded as a way to reduce the costs of noble metals. Accompanying these difficulties and challenges, with the right adjusting and optimizing, Pt-transition metal alloy nanostructures will still be a promising and exciting candidate for low-noble metal electrocatalyst.

Funding: This work was supported by the National Natural Science Foundation of China (Grant No. 11674023), 111 Project (No. B170003), and Fundamental Research Funds for the Central Universities (FRF-TP-17-072A1).

Conflicts of Interest: The authors declare no conflict of interest.

References

1. Sulaiman, N.; Hannan, M.A.; Mohamed, A.; Majlan, E.H.; Daud, W.R.W. A review on energy management system for fuel cell hybrid electric vehicle: Issues and challenges. *Renew. Sustain. Energy Rev.* **2015**, *52*, 802–814. [[CrossRef](#)]
2. Debe, M.K. Electrocatalyst approaches and challenges for automotive fuel cells. *Nature* **2012**, *486*, 43–51. [[CrossRef](#)] [[PubMed](#)]
3. Liu, Z.C.; Koh, S.; Yu, C.F.; Strasser, P. Synthesis, dealloying, and orr electrocatalysis of pdda-stabilized cu-rich pt alloy nanoparticles. *J. Electrochem. Soc.* **2007**, *154*, B1192–B1199. [[CrossRef](#)]
4. Wang, C.; Chi, M.; Li, D.; van der Vliet, D.; Wang, G.; Lin, Q.; Mitchell, J.F.; More, K.L.; Markovic, N.M.; Stamenkovic, V.R. Synthesis of homogeneous pt-bimetallic nanoparticles as highly efficient electrocatalysts. *ACS Catal.* **2011**, *1*, 1355–1359. [[CrossRef](#)]

5. Greeley, J.; Stephens, I.E.L.; Bondarenko, A.S.; Johansson, T.P.; Hansen, H.A.; Jaramillo, T.F.; Rossmeisl, J.; Chorkendorff, I.; Nørskov, J.K. Alloys of platinum and early transition metals as oxygen reduction electrocatalysts. *Nat. Chem.* **2009**, *1*, 552–556. [[CrossRef](#)] [[PubMed](#)]
6. Yang, H.; Alonso-Vante, N.; Lamy, C.; Akins, D.L. High methanol tolerance of carbon-supported pt-cr alloy nanoparticle electrocatalysts for oxygen reduction. *J. Electrochem. Soc.* **2005**, *152*, A704–A709. [[CrossRef](#)]
7. Kang, Y.; Murray, C.B. Synthesis and electrocatalytic properties of cubic mn–pt nanocrystals (nanocubes). *J. Am. Chem. Soc.* **2010**, *132*, 7568–7569. [[CrossRef](#)] [[PubMed](#)]
8. Miura, A.; Wang, H.; Leonard, B.M.; Abruña, H.D.; DiSalvo, F.J. Synthesis of intermetallic ptzn nanoparticles by reaction of pt nanoparticles with zn vapor and their application as fuel cell catalysts. *Chem. Mater.* **2009**, *21*, 2661–2667. [[CrossRef](#)]
9. Strasser, P.; Koh, S.; Anniyev, T.; Greeley, J.; More, K.; Yu, C.; Liu, Z.; Kaya, S.; Nordlund, D.; Ogasawara, H.; et al. Lattice-strain control of the activity in dealloyed core–shell fuel cell catalysts. *Nat. Chem.* **2010**, *2*, 454–460. [[CrossRef](#)] [[PubMed](#)]
10. Ghoshal, S.; Jia, Q.; Bates, M.K.; Li, J.; Xu, C.; Gath, K.; Yang, J.; Waldecker, J.; Che, H.; Liang, W.; et al. Tuning nb–pt interactions to facilitate fuel cell electrocatalysis. *ACS Catal.* **2017**, *7*, 4936–4946. [[CrossRef](#)]
11. Zhang, J.; Yang, H.Z.; Fang, J.Y.; Zou, S.Z. Synthesis and oxygen reduction activity of shape-controlled pt₃ni nanopolyhedra. *Nano Lett.* **2010**, *10*, 638–644. [[CrossRef](#)] [[PubMed](#)]
12. Deng, Y.J.; Tian, N.; Zhou, Z.Y.; Huang, R.; Liu, Z.L.; Xiao, J.; Sun, S.G. Alloy tetrahedral pd–pt catalysts: Enhancing significantly the catalytic activity by synergy effect of high-index facets and electronic structure. *Chem. Sci.* **2012**, *3*, 1157–1161. [[CrossRef](#)]
13. Wang, X.; Figueroa-Cosme, L.; Yang, X.; Luo, M.; Liu, J.Y.; Xie, Z.X.; Xia, Y.N. Pt-based icosahedral nanocages: Using a combination of {111} facets, twin defects, and ultrathin walls to greatly enhance their activity toward oxygen reduction. *Nano Lett.* **2016**, *16*, 1467–1471. [[CrossRef](#)] [[PubMed](#)]
14. Jia, Y.Y.; Jiang, Y.Q.; Zhang, J.W.; Zhang, L.; Chen, Q.L.; Xie, Z.X.; Zheng, L.S. Unique excavated rhombic dodecahedral ptcu₃ alloy nanocrystals constructed with ultrathin nanosheets of high-energy {110} facets. *J. Am. Chem. Soc.* **2014**, *136*, 3748–3751. [[CrossRef](#)] [[PubMed](#)]
15. Huang, X.Q.; Zhao, Z.P.; Fan, J.M.; Tan, Y.M.; Zheng, N.F. Amine-assisted synthesis of concave polyhedral platinum nanocrystals having {411} high-index facets. *J. Am. Chem. Soc.* **2011**, *133*, 4718–4721. [[CrossRef](#)] [[PubMed](#)]
16. Sun, Q.; Ren, Z.; Wang, R.M.; Wang, N.; Cao, X. Platinum catalyzed growth of nipt hollow spheres with an ultrathin shell. *J. Mater. Chem.* **2011**, *21*, 1925–1930. [[CrossRef](#)]
17. Shan, A.X.; Chen, Z.C.; Li, B.Q.; Chen, C.P.; Wang, R.M. Monodispersed, ultrathin nipt hollow nanospheres with tunable diameter and composition via a green chemical synthesis. *J. Mater. Chem. A* **2015**, *3*, 1031–1036. [[CrossRef](#)]
18. Shan, A.X.; Cheng, M.; Fan, H.S.; Chen, Z.C.; Wang, R.M.; Chen, C.P. Nipt hollow nanocatalyst: Green synthesis, size control and electrocatalysis. *Prog. Nat. Sci.* **2014**, *24*, 175–178. [[CrossRef](#)]
19. Sun, Q.; Liu, W.; Wang, R.M. Double-layered nipt nanobowls with ultrathin shell synthesized in water at room temperature. *CrystEngComm* **2012**, *14*, 5151–5154. [[CrossRef](#)]
20. Fan, H.; Cheng, M.; Wang, Z.; Wang, R. Layer-controlled pt–ni porous nanobowls with enhanced electrocatalytic performance. *Nano Res.* **2016**, *10*, 187–198. [[CrossRef](#)]
21. Liu, J.L.; Xia, T.Y.; Wang, S.G.; Yang, G.; Dong, B.W.; Wang, C.; Ma, Q.D.; Sun, Y.; Wang, R.M. Oriented-assembly of hollow fept nanochains with tunable catalytic and magnetic properties. *Nanoscale* **2016**, *8*, 11432–11440. [[CrossRef](#)] [[PubMed](#)]
22. Sun, Q.; Wang, S.G.; Wang, R.M. Well-aligned copt hollow nanochains synthesized in water at room temperature. *J. Phys. Chem. C* **2012**, *116*, 5352–5357. [[CrossRef](#)]
23. Bu, L.Z.; Ding, J.B.; Guo, S.J.; Zhang, X.; Su, D.; Zhu, X.; Yao, J.L.; Guo, J.; Lu, G.; Huang, X.Q. A general method for multimetallic platinum alloy nanowires as highly active and stable oxygen reduction catalysts. *Adv. Mater.* **2015**, *27*, 7204–7212. [[CrossRef](#)] [[PubMed](#)]
24. Cao, Z.; Chen, Q.; Zhang, J.; Li, H.; Jiang, Y.; Shen, S.; Fu, G.; Lu, B.A.; Xie, Z.; Zheng, L. Platinum–nickel alloy excavated nano-multipods with hexagonal close-packed structure and superior activity towards hydrogen evolution reaction. *Nat. Commun.* **2017**, *8*, 15131. [[CrossRef](#)] [[PubMed](#)]

25. Cao, Z.; Li, H.; Zhan, C.; Zhang, J.; Wang, W.; Xu, B.; Lu, F.; Jiang, Y.; Xie, Z.; Zheng, L. Monocrystalline platinum-nickel branched nanocages with enhanced catalytic performance towards the hydrogen evolution reaction. *Nanoscale* **2018**, *10*, 5072–5077. [[CrossRef](#)] [[PubMed](#)]
26. Bu, L.; Guo, S.; Zhang, X.; Shen, X.; Su, D.; Lu, G.; Zhu, X.; Yao, J.; Guo, J.; Huang, X. Surface engineering of hierarchical platinum-cobalt nanowires for efficient electrocatalysis. *Nat. Commun.* **2016**, *7*, 11850. [[CrossRef](#)] [[PubMed](#)]
27. Xu, G.R.; Bai, J.; Jiang, J.X.; Lee, J.M.; Chen, Y. Polyethyleneimine functionalized platinum superstructures: Enhancing hydrogen evolution performance by morphological and interfacial control. *Chem. Sci.* **2017**, *8*, 8411–8418. [[CrossRef](#)] [[PubMed](#)]
28. Gilroy, K.D.; Ruditskiy, A.; Peng, H.-C.; Qin, D.; Xia, Y. Bimetallic nanocrystals: Syntheses, properties, and applications. *Chem. Rev.* **2016**, *116*, 10414–10472. [[CrossRef](#)] [[PubMed](#)]
29. Sui, S.; Wang, X.Y.; Zhou, X.T.; Su, Y.H.; Riffat, S.; Liu, C.J. A comprehensive review of pt electrocatalysts for the oxygen reduction reaction: Nanostructure, activity, mechanism and carbon support in pem fuel cells. *J. Mater. Chem. A* **2017**, *5*, 1808–1825. [[CrossRef](#)]
30. Kaito, T.; Tanaka, H.; Mitsumoto, H.; Sugawara, S.; Shinohara, K.; Ariga, H.; Uehara, H.; Takakusagi, S.; Asakura, K. In situ x-ray absorption fine structure analysis of ptco, ptcu, and ptni alloy electrocatalysts: The correlation of enhanced oxygen reduction reaction activity and structure. *J. Phys. Chem. C* **2016**, *120*, 11519–11527. [[CrossRef](#)]
31. Ogihara, Y.; Yano, H.; Matsumoto, T.; Tryk, D.; Iiyama, A.; Uchida, H. In situ ftir analysis of co-tolerance of a pt-fe alloy with stabilized pt skin layers as a hydrogen anode catalyst for polymer electrolyte fuel cells. *Catalysts* **2016**, *7*, 8. [[CrossRef](#)]
32. Zhao, X.; Takao, S.; Higashi, K.; Kaneko, T.; Samjeskè, G.; Sekizawa, O.; Sakata, T.; Yoshida, Y.; Uruga, T.; Iwasawa, Y. Simultaneous improvements in performance and durability of an octahedral ptnix/c electrocatalyst for next-generation fuel cells by continuous, compressive, and concave pt skin layers. *ACS Catal.* **2017**, *7*, 4642–4654. [[CrossRef](#)]
33. Beermann, V.; Gocyla, M.; Kühl, S.; Padgett, E.; Schmies, H.; Goerlin, M.; Erini, N.; Shviro, M.; Heggen, M.; Dunin-Borkowski, R.E.; et al. Tuning the electrocatalytic oxygen reduction reaction activity and stability of shape-controlled pt–ni nanoparticles by thermal annealing—Elucidating the surface atomic structural and compositional changes. *J. Am. Chem. Soc.* **2017**, *139*, 16536–16547. [[CrossRef](#)] [[PubMed](#)]
34. Han, B.; Carlton, C.E.; Suntivich, J.; Xu, Z.; Shao-Horn, Y. Oxygen reduction activity and stability trends of bimetallic pt_{0.5}m_{0.5} nanoparticle in acid. *J. Phys. Chem. C* **2015**, *119*, 3971–3978. [[CrossRef](#)]
35. Jia, Q.; Li, J.; Caldwell, K.; Ramaker, D.E.; Ziegelbauer, J.M.; Kukreja, R.S.; Kongkanand, A.; Mukerjee, S. Circumventing metal dissolution induced degradation of pt-alloy catalysts in proton exchange membrane fuel cells: Revealing the asymmetric volcano nature of redox catalysis. *ACS Catal.* **2016**, *6*, 928–938. [[CrossRef](#)]
36. Jia, Q.; Liang, W.; Bates, M.K.; Mani, P.; Lee, W.; Mukerjee, S. Activity descriptor identification for oxygen reduction on platinum-based bimetallic nanoparticles: In situ observation of the linear composition–strain–activity relationship. *ACS Nano* **2015**, *9*, 387–400. [[CrossRef](#)] [[PubMed](#)]
37. Sasaki, K.; Naohara, H.; Cai, Y.; Choi, Y.M.; Liu, P.; Vukmirovic, M.B.; Wang, J.X.; Adzic, R.R. Core-protected platinum monolayer shell high-stability electrocatalysts for fuel-cell cathodes. *Angew. Chem.-Int. Ed.* **2010**, *49*, 8602–8607. [[CrossRef](#)] [[PubMed](#)]
38. Wu, J.B.; Yang, H. Platinum-based oxygen reduction electrocatalysts. *Acc. Chem. Res.* **2013**, *46*, 1848–1857. [[CrossRef](#)] [[PubMed](#)]
39. Lee, S.W.; Chen, S.; Sheng, W.; Yabuuchi, N.; Kim, Y.-T.; Mitani, T.; Vescovo, E.; Shao-Horn, Y. Roles of surface steps on pt nanoparticles in electro-oxidation of carbon monoxide and methanol. *J. Am. Chem. Soc.* **2009**, *131*, 15669–15677. [[CrossRef](#)] [[PubMed](#)]
40. Yu, T.; Kim, D.Y.; Zhang, H.; Xia, Y. Platinum concave nanocubes with high-index facets and their enhanced activity for oxygen reduction reaction. *Angew. Chem. Int. Ed.* **2011**, *50*, 2773–2777. [[CrossRef](#)] [[PubMed](#)]
41. Wang, Y.-J.; Long, W.; Wang, L.; Yuan, R.; Ignaszak, A.; Fang, B.; Wilkinson, D.P. Unlocking the door to highly active orr catalysts for pemfc applications: Polyhedron-engineered pt-based nanocrystals. *Energy Environ. Sci.* **2018**, *11*, 258–275. [[CrossRef](#)]

42. Sun, X.; Jiang, K.; Zhang, N.; Guo, S.; Huang, X. Crystalline control of {111} bounded pt₃cu nanocrystals: Multiply-twinned pt₃cu icosahedra with enhanced electrocatalytic properties. *ACS Nano* **2015**, *9*, 7634–7640. [[CrossRef](#)] [[PubMed](#)]
43. Wu, J.; Zhang, J.; Peng, Z.; Yang, S.; Wagner, F.T.; Yang, H. Truncated octahedral pt₃ni oxygen reduction reaction electrocatalysts. *J. Am. Chem. Soc.* **2010**, *132*, 4984–4985. [[CrossRef](#)] [[PubMed](#)]
44. Mourdikoudis, S.; Liz-Marzán, L.M. Oleylamine in nanoparticle synthesis. *Chem. Mater.* **2013**, *25*, 1465–1476. [[CrossRef](#)]
45. Zhang, J.; Fang, J. A general strategy for preparation of pt 3d-transition metal (co, fe, ni) nanocubes. *J. Am. Chem. Soc.* **2009**, *131*, 18543–18547. [[CrossRef](#)] [[PubMed](#)]
46. Choi, S.I.; Xie, S.; Shao, M.; Odell, J.H.; Lu, N.; Peng, H.C.; Protsailo, L.; Guerrero, S.; Park, J.; Xia, X.; et al. Synthesis and characterization of 9 nm pt-ni octahedra with a record high activity of 3.3 a/mg(pt) for the oxygen reduction reaction. *Nano Lett.* **2013**, *13*, 3420–3425. [[CrossRef](#)] [[PubMed](#)]
47. Cui, C.; Gan, L.; Li, H.H.; Yu, S.H.; Heggen, M.; Strasser, P. Octahedral pt₃ni nanoparticle catalysts: Exceptional oxygen reduction activity by tuning the alloy particle surface composition. *Nano Lett.* **2012**, *12*, 5885–5889. [[CrossRef](#)] [[PubMed](#)]
48. Kakade, B.A.; Tamaki, T.; Ohashi, H.; Yamaguchi, T. Highly active bimetallic pdpt and copt nanocrystals for methanol electro-oxidation. *J. Phys. Chem. C* **2012**, *116*, 7464–7470. [[CrossRef](#)]
49. Kang, Y.; Pyo, J.B.; Ye, X.; Gordon, T.R.; Murray, C.B. Synthesis, shape control, and methanol electro-oxidation properties of pt–zn alloy and pt₃zn intermetallic nanocrystals. *ACS Nano* **2012**, *6*, 5642–5647. [[CrossRef](#)] [[PubMed](#)]
50. Xia, T.; Liu, J.; Wang, S.; Wang, C.; Sun, Y.; Gu, L.; Wang, R. Enhanced catalytic activities of nipt truncated octahedral nanoparticles toward ethylene glycol oxidation and oxygen reduction in alkaline electrolyte. *ACS Appl. Mater. Interfaces* **2016**, *8*, 10841–10849. [[CrossRef](#)] [[PubMed](#)]
51. Wu, J.; Qi, L.; You, H.; Gross, A.; Li, J.; Yang, H. Icosahedral platinum alloy nanocrystals with enhanced electrocatalytic activities. *J. Am. Chem. Soc.* **2012**, *134*, 11880–11883. [[CrossRef](#)] [[PubMed](#)]
52. Chen, Q.; Cao, Z.; Du, G.; Kuang, Q.; Huang, J.; Xie, Z.; Zheng, L. Excavated octahedral pt-co alloy nanocrystals built with ultrathin nanosheets as superior multifunctional electrocatalysts for energy conversion applications. *Nano Energy* **2017**, *39*, 582–589. [[CrossRef](#)]
53. Xu, H.; Song, P.; Wang, J.; Du, Y. Shape-controlled synthesis of platinum–copper nanocrystals for efficient liquid fuel electrocatalysis. *Langmuir* **2018**, *34*, 7981–7988. [[CrossRef](#)] [[PubMed](#)]
54. Xia, B.Y.; Wu, H.B.; Wang, X.; Lou, X.W. One-pot synthesis of cubic ptcu₃ nanocages with enhanced electrocatalytic activity for the methanol oxidation reaction. *J. Am. Chem. Soc.* **2012**, *134*, 13934–13937. [[CrossRef](#)] [[PubMed](#)]
55. Chen, C.; Kang, Y.; Huo, Z.; Zhu, Z.; Huang, W.; Xin, H.L.; Snyder, J.D.; Li, D.; Herron, J.A.; Mavrikakis, M.; et al. Highly crystalline multimetallic nanoframes with three-dimensional electrocatalytic surfaces. *Science* **2014**, *343*, 1339–1343. [[CrossRef](#)] [[PubMed](#)]
56. Becknell, N.; Son, Y.; Kim, D.; Li, D.; Yu, Y.; Niu, Z.; Lei, T.; Sneed, B.T.; More, K.L.; Markovic, N.M.; et al. Control of architecture in rhombic dodecahedral pt–ni nanoframe electrocatalysts. *J. Am. Chem. Soc.* **2017**, *139*, 11678–11681. [[CrossRef](#)] [[PubMed](#)]
57. Ding, J.; Bu, L.; Guo, S.; Zhao, Z.; Zhu, E.; Huang, Y.; Huang, X. Morphology and phase controlled construction of pt-ni nanostructures for efficient electrocatalysis. *Nano Lett.* **2016**, *16*, 2762–2767. [[CrossRef](#)] [[PubMed](#)]
58. Zhang, S.; Zhang, X.; Jiang, G.; Zhu, H.; Guo, S.; Su, D.; Lu, G.; Sun, S. Tuning nanoparticle structure and surface strain for catalysis optimization. *J. Am. Chem. Soc.* **2014**, *136*, 7734–7739. [[CrossRef](#)] [[PubMed](#)]
59. Han, B.; Carlton, C.E.; Kongkanand, A.; Kukreja, R.S.; Theobald, B.R.; Gan, L.; O'Malley, R.; Strasser, P.; Wagner, F.T.; Shao-Horn, Y. Record activity and stability of dealloyed bimetallic catalysts for proton exchange membrane fuel cells. *Energy Environ. Sci.* **2015**, *8*, 258–266. [[CrossRef](#)]
60. Zhang, S.; Hao, Y.; Su, D.; Doan-Nguyen, V.V.T.; Wu, Y.; Li, J.; Sun, S.; Murray, C.B. Monodisperse core/shell ni/fept nanoparticles and their conversion to ni/pt to catalyze oxygen reduction. *J. Am. Chem. Soc.* **2014**, *136*, 15921–15924. [[CrossRef](#)] [[PubMed](#)]

61. Shan, A.; Chen, C.; Zhang, W.; Cheng, D.; Shen, X.; Yu, R.; Wang, R. Giant enhancement and anomalous temperature dependence of magnetism in monodispersed nipt₂ nanoparticles. *Nano Res.* **2017**, *10*, 3238–3247. [[CrossRef](#)]
62. Ghosh, T.; Vukmirovic, M.B.; DiSalvo, F.J.; Adzic, R.R. Intermetallics as novel supports for pt monolayer o₂ reduction electrocatalysts: Potential for significantly improving properties. *J. Am. Chem. Soc.* **2010**, *132*, 906–907. [[CrossRef](#)] [[PubMed](#)]
63. Xie, S.F.; Choi, S.I.; Lu, N.; Roling, L.T.; Herron, J.A.; Zhang, L.; Park, J.; Wang, J.G.; Kim, M.J.; Xie, Z.X.; et al. Atomic layer-by-layer deposition of pt on pd nanocubes for catalysts with enhanced activity and durability toward oxygen reduction. *Nano Lett.* **2014**, *14*, 3570–3576. [[CrossRef](#)] [[PubMed](#)]
64. Oezaslan, M.; Hasché, F.; Strasser, P. Pt-based core–shell catalyst architectures for oxygen fuel cell electrodes. *J. Phys. Chem. Lett.* **2013**, *4*, 3273–3291. [[CrossRef](#)]
65. Fu, S.F.; Zhu, C.Z.; Song, J.H.; Engelhard, M.H.; He, Y.; Du, D.; Wang, C.M.; Lin, Y.H. Three-dimensional pt_{ni} hollow nanochains as an enhanced electrocatalyst for the oxygen reduction reaction. *J. Mater. Chem. A* **2016**, *4*, 8755–8761. [[CrossRef](#)]
66. Serrà, A.; Gómez, E.; Vallés, E. Facile electrochemical synthesis, using microemulsions with ionic liquid, of highly mesoporous co_{pt} nanorods with enhanced electrocatalytic performance for clean energy. *Int. J. Hydrogen Energy* **2015**, *40*, 8062–8070. [[CrossRef](#)]
67. Guo, L.; Huang, L.B.; Jiang, W.J.; Wei, Z.D.; Wan, L.J.; Hu, J.S. Tuning the branches and composition of pt_{cu} nanodendrites through underpotential deposition of cu towards advanced electrocatalytic activity. *J. Mater. Chem. A* **2017**, *5*, 9014–9021. [[CrossRef](#)]
68. Li, H.-H.; Fu, Q.-Q.; Xu, L.; Ma, S.-Y.; Zheng, Y.-R.; Liu, X.-J.; Yu, S.-H. Highly crystalline pt_{cu} nanotubes with three dimensional molecular accessible and restructured surface for efficient catalysis. *Energy Environ. Sci.* **2017**, *10*, 1751–1756. [[CrossRef](#)]
69. Xia, Z.; Zhang, P.; Feng, G.; Xia, D.; Zhang, J. Crossed pt_{co}cu alloy nanocrystals with high-index facets as highly active catalyst for methanol oxidation reaction. *Adv. Mater. Interfaces* **2018**, *5*, 1800297. [[CrossRef](#)]
70. Zhang, P.; Dai, X.; Zhang, X.; Chen, Z.; Yang, Y.; Sun, H.; Wang, X.; Wang, H.; Wang, M.; Su, H.; et al. One-pot synthesis of ternary pt–ni–cu nanocrystals with high catalytic performance. *Chem. Mater.* **2015**, *27*, 6402–6410. [[CrossRef](#)]
71. Moseley, P.; Curtin, W.A. Computational design of strain in core–shell nanoparticles for optimizing catalytic activity. *Nano Lett.* **2015**, *15*, 4089–4095. [[CrossRef](#)] [[PubMed](#)]
72. Bu, L.; Zhang, N.; Guo, S.; Zhang, X.; Li, J.; Yao, J.; Wu, T.; Lu, G.; Ma, J.Y.; Su, D.; et al. Biaxially strained pt_{pb}/pt core/shell nanoplate boosts oxygen reduction catalysis. *Science* **2016**, *354*, 1410–1414. [[CrossRef](#)] [[PubMed](#)]
73. Gan, L.; Heggen, M.; Rudi, S.; Strasser, P. Core-shell compositional fine structures of dealloyed pt(x)ni(1-x) nanoparticles and their impact on oxygen reduction catalysis. *Nano Lett.* **2012**, *12*, 5423–5430. [[CrossRef](#)] [[PubMed](#)]
74. Jia, Q.; Caldwell, K.; Strickland, K.; Ziegelbauer, J.M.; Liu, Z.; Yu, Z.; Ramaker, D.E.; Mukerjee, S. Improved oxygen reduction activity and durability of dealloyed pt_{co} x catalysts for proton exchange membrane fuel cells: Strain, ligand, and particle size effects. *ACS Catal.* **2015**, *5*, 176–186. [[CrossRef](#)] [[PubMed](#)]
75. Mayrhofer, K.J.J.; Juhart, V.; Hartl, K.; Hanzlik, M.; Arenz, M. Adsorbate-induced surface segregation for core–shell nanocatalysts. *Angew. Chem. Int. Ed.* **2009**, *48*, 3529–3531. [[CrossRef](#)] [[PubMed](#)]
76. Prabhudev, S.; Bugnet, M.; Zhu, G.Z.; Bock, C.; Botton, G.A. Surface segregation of fe in pt-fe alloy nanoparticles: Its precedence and effect on the ordered-phase evolution during thermal annealing. *ChemCatChem* **2015**, *7*, 3655–3664. [[CrossRef](#)] [[PubMed](#)]
77. Zhang, Z.-C.; Tian, X.-C.; Zhang, B.-W.; Huang, L.; Zhu, F.-C.; Qu, X.-M.; Liu, L.; Liu, S.; Jiang, Y.-X.; Sun, S.-G. Engineering phase and surface composition of pt₃co nanocatalysts: A strategy for enhancing co tolerance. *Nano Energy* **2017**, *34*, 224–232. [[CrossRef](#)]
78. Wang, R.; Tao, J.; Du, K.; Wang, Y.; Ge, B.; Li, F.; Liu, W.; Wu, L.; Liu, H.; Zhang, Y.; et al. Transmission electron microscopy. In *Progress in Nanoscale Characterization and Manipulation*; Wang, R., Wang, C., Zhang, H., Tao, J., Bai, X., Eds.; Springer: Singapore, 2018; pp. 69–203.
79. Zhang, L.; Shi, W.; Zhang, B. A review of electrocatalyst characterization by transmission electron microscopy. *J. Energy Chem.* **2017**, *26*, 1117–1135. [[CrossRef](#)]

80. Gocyla, M.; Kuehl, S.; Shviro, M.; Heyen, H.; Selve, S.; Dunin-Borkowski, R.E.; Heggen, M.; Strasser, P. Shape stability of octahedral ptni nanocatalysts for electrochemical oxygen reduction reaction studied by in situ transmission electron microscopy. *ACS Nano* **2018**, *12*, 5306–5311. [[CrossRef](#)] [[PubMed](#)]
81. Ma, Y.; Gao, W.; Shan, H.; Chen, W.; Shang, W.; Tao, P.; Song, C.; Addiego, C.; Deng, T.; Pan, X.; et al. Platinum-based nanowires as active catalysts toward oxygen reduction reaction: In situ observation of surface-diffusion-assisted, solid-state oriented attachment. *Adv. Mater.* **2017**, *29*, 1703460. [[CrossRef](#)] [[PubMed](#)]
82. Liu, J.; Liu, W.; Sun, Q.; Wang, S.; Sun, K.; Schwank, J.; Wang, R. In situ tracing of atom migration in pt/nipt hollow spheres during catalysis of co oxidation. *Chem. Commun.* **2014**, *50*, 1804–1807. [[CrossRef](#)] [[PubMed](#)]
83. Duan, S.B.; Wang, R.M.; Liu, J.Y. Stability investigation of a high number density pt-1/fe2o3 single-atom catalyst under different gas environments by haadf-stem. *Nanotechnology* **2018**, *29*, 204002. [[CrossRef](#)] [[PubMed](#)]
84. Luo, L.; Engelhard, M.H.; Shao, Y.; Wang, C. Revealing the dynamics of platinum nanoparticle catalysts on carbon in oxygen and water using environmental tem. *ACS Catal.* **2017**, *7*, 7658–7664. [[CrossRef](#)]
85. Hodnik, N.; Dehm, G.; Mayrhofer, K.J. Importance and challenges of electrochemical in situ liquid cell electron microscopy for energy conversion research. *Acc. Chem. Res.* **2016**, *49*, 2015–2022. [[CrossRef](#)] [[PubMed](#)]
86. Liu, X.L.; Wood, J.D.; Chen, K.S.; Cho, E.; Hersam, M.C. In situ thermal decomposition of exfoliated two-dimensional black phosphorus. *J. Phys. Chem. Lett.* **2015**, *6*, 773–778. [[CrossRef](#)] [[PubMed](#)]
87. Becknell, N.; Kang, Y.; Chen, C.; Resasco, J.; Kornienko, N.; Guo, J.; Markovic, N.M.; Somorjai, G.A.; Stamenkovic, V.R.; Yang, P. Atomic structure of pt3ni nanoframe electrocatalysts by in situ x-ray absorption spectroscopy. *J. Am. Chem. Soc.* **2015**, *137*, 15817–15824. [[CrossRef](#)] [[PubMed](#)]
88. Petkov, V.; Maswadeh, Y.; Lu, A.; Shan, S.; Kareem, H.; Zhao, Y.; Luo, J.; Zhong, C.-J.; Beyer, K.; Chapman, K. Evolution of active sites in pt-based nanoalloy catalysts for the oxidation of carbonaceous species by combined in situ infrared spectroscopy and total x-ray scattering. *ACS Appl. Mater. Interfaces* **2018**, *10*, 10870–10881. [[CrossRef](#)] [[PubMed](#)]
89. Avanesian, T.; Dai, S.; Kale, M.J.; Graham, G.W.; Pan, X.; Christopher, P. Quantitative and atomic-scale view of co-induced pt nanoparticle surface reconstruction at saturation coverage via dft calculations coupled with in situ tem and ir. *J. Am. Chem. Soc.* **2017**, *139*, 4551–4558. [[CrossRef](#)] [[PubMed](#)]
90. Stamenkovic, V.; Mun, B.S.; Mayrhofer, K.J.J.; Ross, P.N.; Markovic, N.M.; Rossmeisl, J.; Greeley, J.; Nørskov, J.K. Changing the activity of electrocatalysts for oxygen reduction by tuning the surface electronic structure. *Angew. Chem. Int. Ed.* **2006**, *45*, 2897–2901. [[CrossRef](#)] [[PubMed](#)]
91. Greeley, J.; Mavrikakis, M. Alloy catalysts designed from first principles. *Nat. Mater.* **2004**, *3*, 810–815. [[CrossRef](#)] [[PubMed](#)]
92. Stamenkovic, V.R.; Mun, B.S.; Arenz, M.; Mayrhofer, K.J.J.; Lucas, C.A.; Wang, G.; Ross, P.N.; Markovic, N.M. Trends in electrocatalysis on extended and nanoscale pt-bimetallic alloy surfaces. *Nat. Mater.* **2007**, *6*, 241–247. [[CrossRef](#)] [[PubMed](#)]
93. Stamenkovic, V.R.; Fowler, B.; Mun, B.S.; Wang, G.; Ross, P.N.; Lucas, C.A.; Marković, N.M. Improved oxygen reduction activity on pt3ni(111) via increased surface site availability. *Science* **2007**, *315*, 493–497. [[CrossRef](#)] [[PubMed](#)]
94. Choi, J.; Jang, J.-H.; Roh, C.-W.; Yang, S.; Kim, J.; Lim, J.; Yoo, S.J.; Lee, H. Gram-scale synthesis of highly active and durable octahedral ptni nanoparticle catalysts for proton exchange membrane fuel cell. *Appl. Catal. B Environ.* **2018**, *225*, 530–537. [[CrossRef](#)]
95. Godínez-Salomón, F.; Mendoza-Cruz, R.; Arellano-Jimenez, M.J.; Jose-Yacamán, M.; Rhodes, C.P. Metallic two-dimensional nanoframes: Unsupported hierarchical nickel–platinum alloy nanoarchitectures with enhanced electrochemical oxygen reduction activity and stability. *ACS Appl. Mater. Interfaces* **2017**, *9*, 18660–18674. [[CrossRef](#)] [[PubMed](#)]
96. Wang, Q.; Chen, S.; Shi, F.; Chen, K.; Nie, Y.; Wang, Y.; Wu, R.; Li, J.; Zhang, Y.; Ding, W.; et al. Structural evolution of solid pt nanoparticles to a hollow ptf alloy with a pt-skin surface via space-confined pyrolysis and the nanoscale kirkendall effect. *Adv. Mater.* **2016**, *28*, 10673–10678. [[CrossRef](#)] [[PubMed](#)]
97. Yang, K.; Jiang, P.; Chen, J.; Chen, Q. Nanoporous ptf nanoparticles supported on n-doped porous carbon sheets derived from metal-organic frameworks as highly efficient and durable oxygen reduction reaction catalysts. *ACS Appl. Mater. Interfaces* **2017**, *9*, 32106–32113. [[CrossRef](#)] [[PubMed](#)]

98. Dhavale, V.M.; Kurungot, S. Cu–Pt nanocage with 3-d electrocatalytic surface as an efficient oxygen reduction electrocatalyst for a primary Zn–air battery. *ACS Catal.* **2015**, *5*, 1445–1452. [[CrossRef](#)]
99. Luo, S.; Tang, M.; Shen, P.K.; Ye, S. Atomic-scale preparation of octopod nanoframes with high-index facets as highly active and stable catalysts. *Adv. Mater.* **2017**, *29*, 1601687. [[CrossRef](#)] [[PubMed](#)]
100. Kwon, H.; Kabiraz, M.K.; Park, J.; Oh, A.; Baik, H.; Choi, S.I.; Lee, K. Dendrite-embedded platinum-nickel multiframe as highly active and durable electrocatalyst toward the oxygen reduction reaction. *Nano Lett.* **2018**, *18*, 2930–2936. [[CrossRef](#)] [[PubMed](#)]
101. Tiwari, J.N.; Tiwari, R.N.; Singh, G.; Kim, K.S. Recent progress in the development of anode and cathode catalysts for direct methanol fuel cells. *Nano Energy* **2013**, *2*, 553–578. [[CrossRef](#)]
102. Tian, X.L.; Wang, L.; Deng, P.; Chen, Y.; Xia, B.Y. Research advances in unsupported Pt-based catalysts for electrochemical methanol oxidation. *J. Energy Chem.* **2017**, *26*, 1067–1076. [[CrossRef](#)]
103. Lu, Y.Z.; Jiang, Y.Y.; Wu, H.B.; Chen, W. Nano-PTPD cubes on graphene exhibit enhanced activity and durability in methanol electrooxidation after CO stripping-cleaning. *J. Phys. Chem. C* **2013**, *117*, 2926–2938. [[CrossRef](#)]
104. Yin, A.X.; Min, X.Q.; Zhang, Y.W.; Yan, C.H. Shape-selective synthesis and facet-dependent enhanced electrocatalytic activity and durability of monodisperse sub-10 nm Pt-Pd tetrahedrons and cubes. *J. Am. Chem. Soc.* **2011**, *133*, 3816–3819. [[CrossRef](#)] [[PubMed](#)]
105. Xia, T.Y.; Liu, J.L.; Wang, S.G.; Wang, C.; Sun, Y.; Wang, R.M. Nanomagnetic CoPt truncated octahedrons: Facile synthesis, superior electrocatalytic activity and stability for methanol oxidation. *Sci. China-Mater.* **2017**, *60*, 57–67. [[CrossRef](#)]
106. Wang, Q.; Zhao, Z.; Jia, Y.; Wang, M.; Qi, W.; Pang, Y.; Yi, J.; Zhang, Y.; Li, Z.; Zhang, Z. Unique Cu@CuPt core-shell concave octahedron with enhanced methanol oxidation activity. *ACS Appl. Mater. Interfaces* **2017**, *9*, 36817–36827. [[CrossRef](#)] [[PubMed](#)]
107. Luo, S.; Shen, P.K. Concave platinum–copper octopod nanoframes bounded with multiple high-index facets for efficient electrooxidation catalysis. *ACS Nano* **2016**, *11*, 11946–11953. [[CrossRef](#)] [[PubMed](#)]
108. Li, C.; Liu, T.; He, T.; Ni, B.; Yuan, Q.; Wang, X. Composition-driven shape evolution to Cu-rich PtCu octahedral alloy nanocrystals as superior bifunctional catalysts for methanol oxidation and oxygen reduction reaction. *Nanoscale* **2018**, *10*, 4670–4674. [[CrossRef](#)] [[PubMed](#)]
109. Zhang, Z.C.; Luo, Z.M.; Chen, B.; Wei, C.; Zhao, L.; Chen, J.Z.; Zhang, X.; Lai, Z.C.; Fan, Z.X.; Tan, C.L.; et al. One-pot synthesis of highly anisotropic five-fold-twinned PtCu nanoframes used as a bifunctional electrocatalyst for oxygen reduction and methanol oxidation. *Adv. Mater.* **2016**, *28*, 8712–8717. [[CrossRef](#)] [[PubMed](#)]
110. Kwon, T.; Jun, M.; Kim, H.Y.; Oh, A.; Park, J.; Baik, H.; Joo, S.H.; Lee, K. Vertex-reinforced PtCuCo ternary nanoframes as efficient and stable electrocatalysts for the oxygen reduction reaction and the methanol oxidation reaction. *Adv. Funct. Mater.* **2018**, *28*, 1706440. [[CrossRef](#)]
111. Liu, T.; Wang, K.; Yuan, Q.; Shen, Z.; Wang, Y.; Zhang, Q.; Wang, X. Monodispersed sub-5.0 nm PtCu nanoalloys as enhanced bifunctional electrocatalysts for oxygen reduction reaction and ethanol oxidation reaction. *Nanoscale* **2017**, *9*, 2963–2968. [[CrossRef](#)] [[PubMed](#)]
112. Mun, Y.; Shim, J.; Kim, K.; Han, J.W.; Kim, S.-K.; Ye, Y.; Hwang, J.; Lee, S.; Jang, J.; Kim, Y.-T.; et al. Direct access to aggregation-free and small intermetallic nanoparticles in ordered, large-pore mesoporous carbon for an electrocatalyst. *RSC Adv.* **2016**, *6*, 88255–88264. [[CrossRef](#)]
113. Huang, H.; Hu, X.; Zhang, J.; Su, N.; Cheng, J. Facile fabrication of platinum-cobalt alloy nanoparticles with enhanced electrocatalytic activity for a methanol oxidation reaction. *Sci. Rep.* **2017**, *7*, 45555. [[CrossRef](#)] [[PubMed](#)]
114. Wang, X.X.; Hwang, S.; Pan, Y.T.; Chen, K.; He, Y.; Karakalos, S.; Zhang, H.; Spendelow, J.S.; Su, D.; Wu, G. Ordered Pt₃Co intermetallic nanoparticles derived from metal-organic frameworks for oxygen reduction. *Nano Lett.* **2018**, *18*, 4163–4171. [[CrossRef](#)] [[PubMed](#)]
115. Ying, J.; Li, J.; Jiang, G.; Cano, Z.P.; Ma, Z.; Zhong, C.; Su, D.; Chen, Z. Metal-organic frameworks derived platinum-cobalt bimetallic nanoparticles in nitrogen-doped hollow porous carbon capsules as a highly active and durable catalyst for oxygen reduction reaction. *Appl. Catal. B Environ.* **2018**, *225*, 496–503. [[CrossRef](#)]
116. Liu, Y.; Chen, L.; Cheng, T.; Guo, H.; Sun, B.; Wang, Y. Preparation and application in assembling high-performance fuel cell catalysts of colloidal PtCu alloy nanoclusters. *J. Power Sources* **2018**, *395*, 66–76. [[CrossRef](#)]

117. Zhang, C.; Zhang, R.; Li, X.; Chen, W. Pt₁ nanocrystals supported on hollow carbon spheres: Enhancing the electrocatalytic performance through high-temperature annealing and electrochemical co stripping treatments. *ACS Appl. Mater. Interfaces* **2017**, *9*, 29623–29632. [[CrossRef](#)] [[PubMed](#)]
118. Wu, Y.; Zhao, Y.; Liu, J.; Wang, F. Adding refractory 5d transition metal w into ptco system: An advanced ternary alloy for efficient oxygen reduction reaction. *J. Mater. Chem. A* **2018**, *6*, 10700–10709. [[CrossRef](#)]
119. Duan, S.; Wang, R. Bimetallic nanostructures with magnetic and noble metals and their physicochemical applications. *Prog. Nat. Sci. Mater. Int.* **2013**, *23*, 113–126. [[CrossRef](#)]



© 2018 by the authors. Licensee MDPI, Basel, Switzerland. This article is an open access article distributed under the terms and conditions of the Creative Commons Attribution (CC BY) license (<http://creativecommons.org/licenses/by/4.0/>).